npj | Microgravity

Sex-specific cardiovascular adaptations to simulated microgravity in Sprague-Dawley rats

Ebrahim Elsangeedy [1,#], Dina N Yamaleyeva [1,#], Nicholas P Edenhoffer [2], Allyson Deak [1], Anna Soloshenko [1], Jonathan Ray [1], Xuming Sun [1], Omar H Shaltout [1], Nildris Cruz-Diaz [1], Brian Westwood [1], Daniel Kim-Shapiro [3], Debra I Diz [1], Shay Soker [2], Victor M Pulgar [1,4], April Ronca [5], Jeffrey S Willey [6], Liliya M Yamaleyeva [1,✉]

Author information   Article notes   Copyright and License information
PMCID: PMC11659408   PMID: 39702444

Abstract

Men and women have different cardiovascular responses to spaceflight; however, few studies have focused on direct comparisons between sexes. We investigated the mechanisms of aortic stiffening in socially and sexually mature 20-week-old male and female Sprague Dawley (SD) rats exposed to hindlimb unloading (HLU) for 14 days. Pulse wave velocity (PWV) was greater in the aortic arch of females after HLU versus control females ($n = 6$–8). HLU had no effect on aortic PWV in males ($n = 5$–6). Aortic α smooth muscle actin, myosin, collagen, elastin, and collagen-to-elastin ratio were not different in rats of either sex following HLU. The levels of G protein-coupled estrogen receptor (GPER) were lower in the aorta of SD females exposed to HLU compared with female controls but were not altered in males. HLU females also had lower aortic PPARγ, increased oxidative stress markers, and diastolic dysfunction compared with control females. GPER agonist G1 prevented the increase in PWV and 8-hydroxy-2'-deoxyguanosine without altering PPARγ or p47phox in HLU females ($n = 4$ in each group) suggesting that lower GPER may contribute to arterial stiffening in the setting of simulated microgravity. This study highlights sex-specific vascular adaptations to the state of
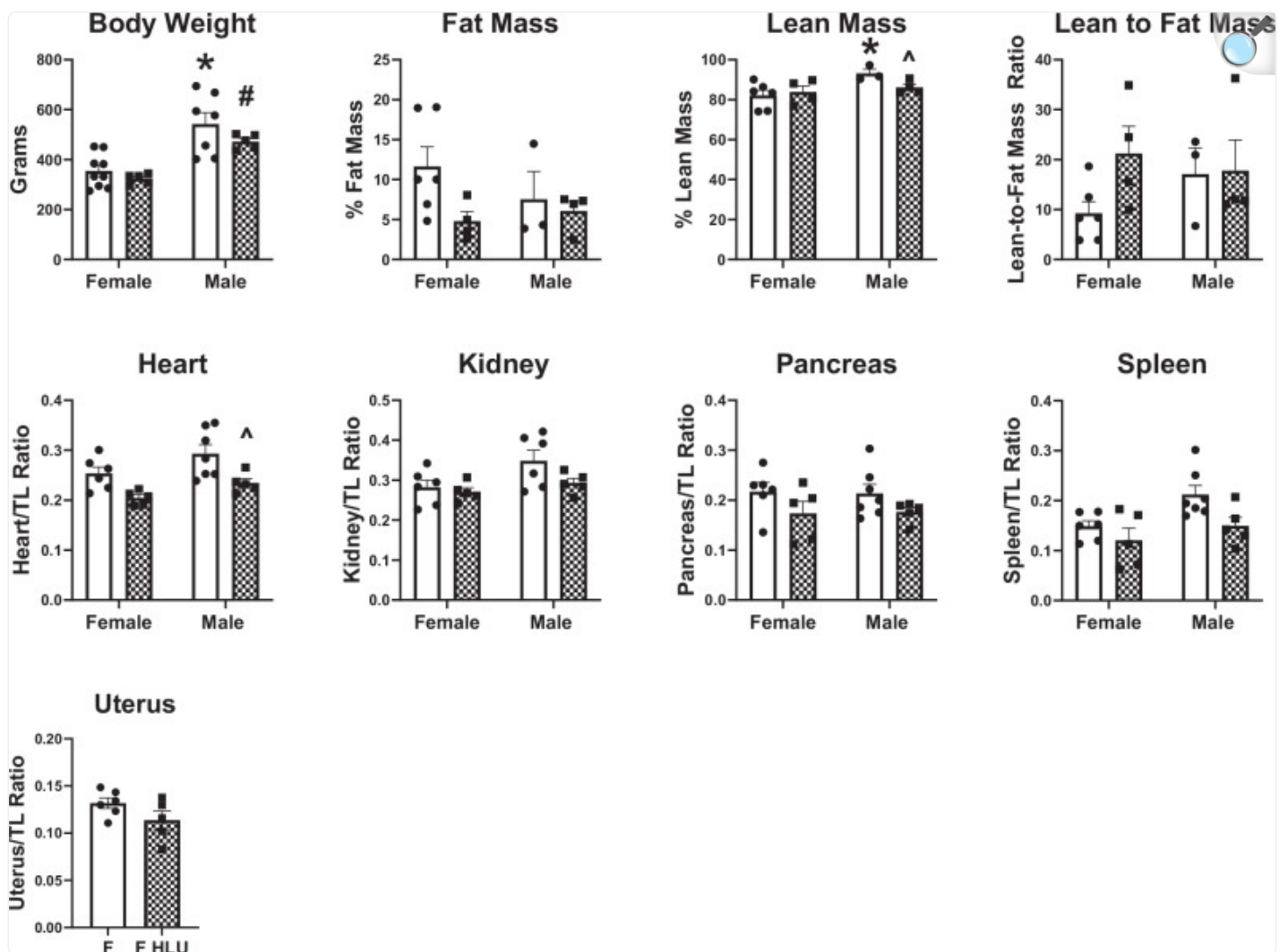
simulated microgravity.

Introduction

The cardiovascular adaptations in astronauts both during and after spaceflight are variable in terms of sex, duration of exposure, and the model used for the studies. Men and women have different recovery mechanisms from stress factors, which can influence the response to the spaceflight environment[1]. Though women are known to be protected against heart disease prior to menopause, responses of the vascular system to spaceflight are complicated by additional stress factors including microgravity, space radiation, inactivity, or isolation. Few studies have focused on the sex differences in the adaptations of the cardiovascular system to spaceflight in spite of the fact that the proportion of women participating in space missions has reached about 10% and continues to increase[2]. The empirically reported effects of spaceflight on the cardiovascular system are varied across people who have been in space[3]. Some common short-term physiological effects of spaceflight include changes in blood volume distribution and alterations in baroreflex function[3]. Prolonged exposure to spaceflight also impacts cardiovascular system including red blood cell count, systemic vascular resistance, stroke volume, and cardiac output[4–7]. Sex-based differences in cardiovascular responses have been reported with changes in both sexes occurring after several weeks in space[1,8]. Female astronauts experience a greater loss of plasma volume while male astronauts appear to be more prone to develop a spaceflight associated neuro-ocular syndrome (SANS)[9–11]. Furthermore, following a 6-month spaceflight, women tended to have greater increases in plasma renin and aldosterone versus men, while both men and women experienced increased carotid artery stiffness[5]. The observed sex differences underscore the importance of understanding the underlying mechanisms of cardiovascular changes and sex-specific adaptations to both terrestrial and space-induced stressors important for the development of personalized preventative countermeasures for astronauts. To better understand the changes in cardiovascular adaptations in response to spaceflight environment, terrestrial studies are focused on recapitulating microgravity in human subjects with head-down tilt (HDT) bed rest or in rodent models with hindlimb unloading (HLU)[12,13]. The mechanisms underlying the cardiovascular system responses and arterial stiffness are not well understood particularly in the female subjects. Furthermore, the majority of HLU studies use male rodent subjects, with even fewer examining differences between sexes. Therefore, the present study investigated the mechanisms underlying the development of central arterial stiffness in female and male Sprague Dawley (SD) rats in response to HLU as an analog for spaceflight-induced microgravity.

Results

Effect of HLU on body weight, organ weight

The body weight of male control rats was significantly ($p < 0.05$) greater than the body weight of female control rats (Fig. 1). Similarly, male HLU rats were heavier than female HLU rats (Fig. 1). To account for this variability in body weight while allowing for comparison between sexes, organ weights (heart, kidney, pancreas, spleen, uterus) were normalized to individual tibia length values that more accurately reflect physiological changes in organ weights[14]. Body composition analysis revealed no differences in total fat mass between study groups, however, control unexposed males had greater lean mass compared with control females (Fig. 1). Exposure to HLU reduced lean mass in males (Fig. 1C). Lean-to-fat mass ratio was not different between study groups (Fig. 1). Within each sex, HLU treatment did not affect organ weights (Fig. 1) except the hearts where male rats exposed to HLU had lower heart weight compared to the male control group (Fig. 1). HLU did not affect uterine weight in female SD rats (Fig. 1).

Fig. 1. The effect of 14-days of HLU on body and organ weights in 20-week-old female and male Sprague-Dawley rats.
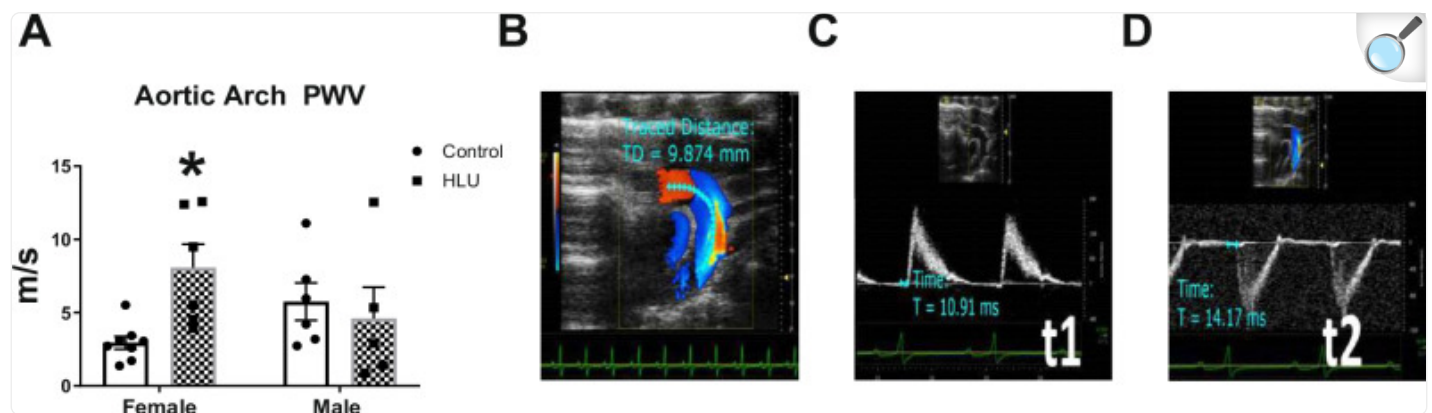
Clear bars indicate control unexposed animals; checkered bars indicate rats exposed to hindlimb unloading (HLU). Data are mean ± SEM, $*p < 0.05$ versus Control Female; $^{\#}p < 0.05$ versus HLU Female; $^{\wedge}p < 0.05$ versus Control Male; $n = 3–9$ per group.

Aortic PWV and cardiac function in response to HLU

The effect of HLU on PWV of the aortic arch in male and female SD rats was determined (Fig. 2). HLU females had a

greater aortic arch PWV compared to control females or HLU males (Fig. 2). No differences were found in PWV in HLU males compared with male controls (Fig. 2). HLU also increased PWV of the left common carotid artery in the female rats compared to female controls (Fig. S1). To determine whether changes in cardiac function could explain differences in PWV caused by HLU exposure, systolic and diastolic function parameters were measured in the female control and HLU rats. Stroke volume and cardiac output were not different between control and HLU female groups (Fig. S2A, B). Although within normal ranges, female HLU rats had increased ejection fraction compared to control female rats (Fig. S2C). Diastolic function, measured by E/E' ratio was worse in HLU female rats versus female controls (Fig. S2D).

Fig. 2. Aortic arch pulse wave velocity (PWV) in female and male rats in response to HLU.
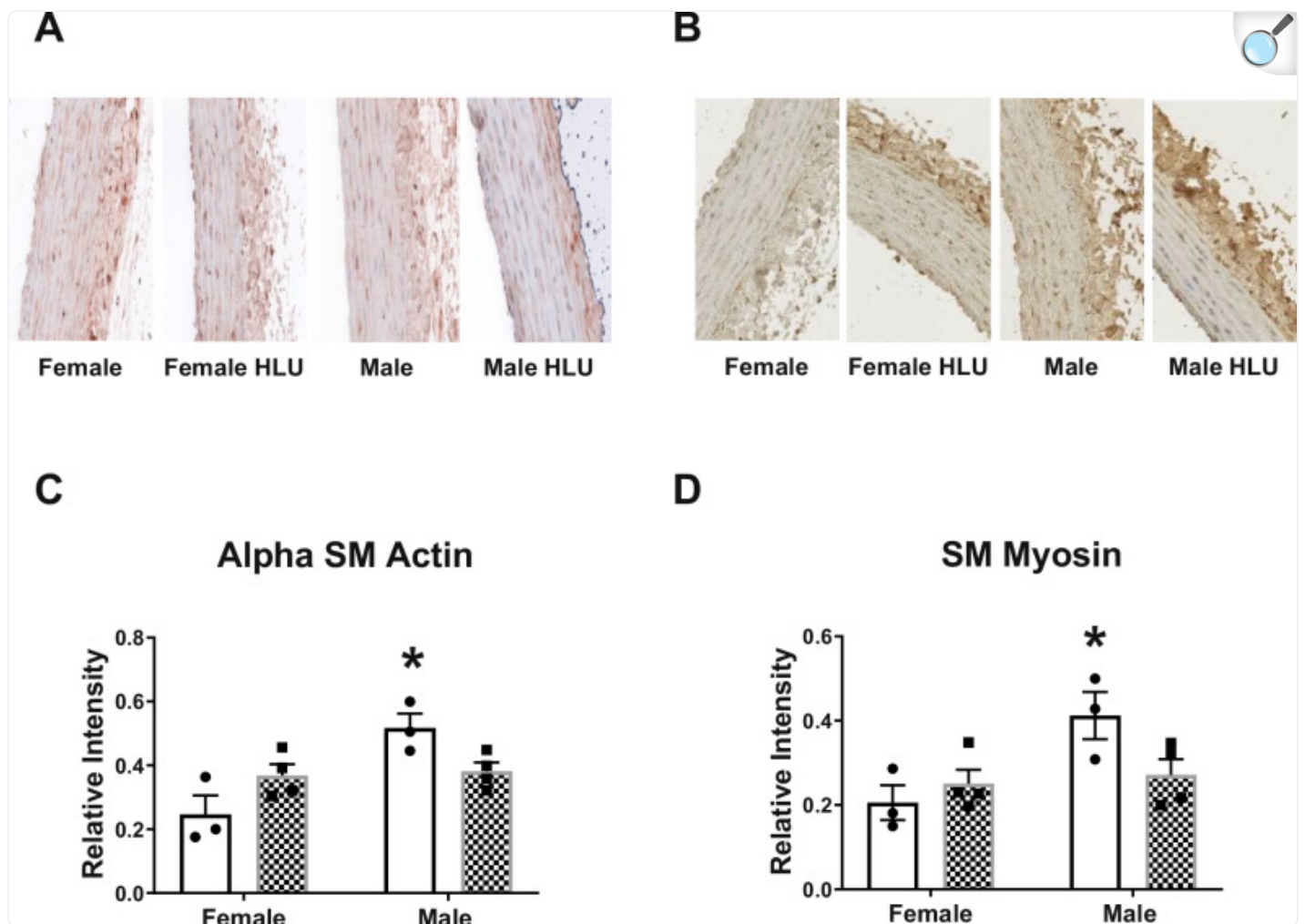

Open in a new tab

Clear bars indicate control unexposed animals; checkered bars indicate rats exposed to hindlimb unloading (HLU) (**A**). Data are mean ± SEM, *$p < 0.05$ versus Control Female; $n = 5–8$ per group. PWV was calculated as PWV = D/pulse transit time Δt, where D is the distance between two points in mm ($t2$ and $t1$) in the aortic arch, and t is the signal transit time estimated between R on electrocardiogram and the beginning of the Doppler wave in ms (**B–D**).

Aortic extracellular matrix (ECM) and contractile components

α-smooth muscle actin and myosin were assessed in the media of aortic arch of female and male rats following HLU exposure (Fig. 3). The aortas of male controls had greater levels of both proteins compared to control females. HLU had no effect on either α-smooth muscle actin or myosin in female or male rats (Fig. 3). Collagen and elastin contents, and collagen-to-elastin ratio were not different in control or HLU female or male rats (Fig. 4).

# Fig. 3. Smooth muscle (SM) contractile protein staining of aortic media.

Representative images and analysis of relative intensity of α-smooth muscle alpha actin (**A**, **C**) and smooth muscle myosin (**B**, **D**) in female and male SD rats with or without HLU exposure are shown. Data are mean ± SEM, *$p < 0.05$, versus Female, $n = 3$–4 per group. Magnification: ×20.

Fig. 4. Effect of HLU on total collagen or elastin area, and collagen-to-elastin ratio in aortic media of SD rats.
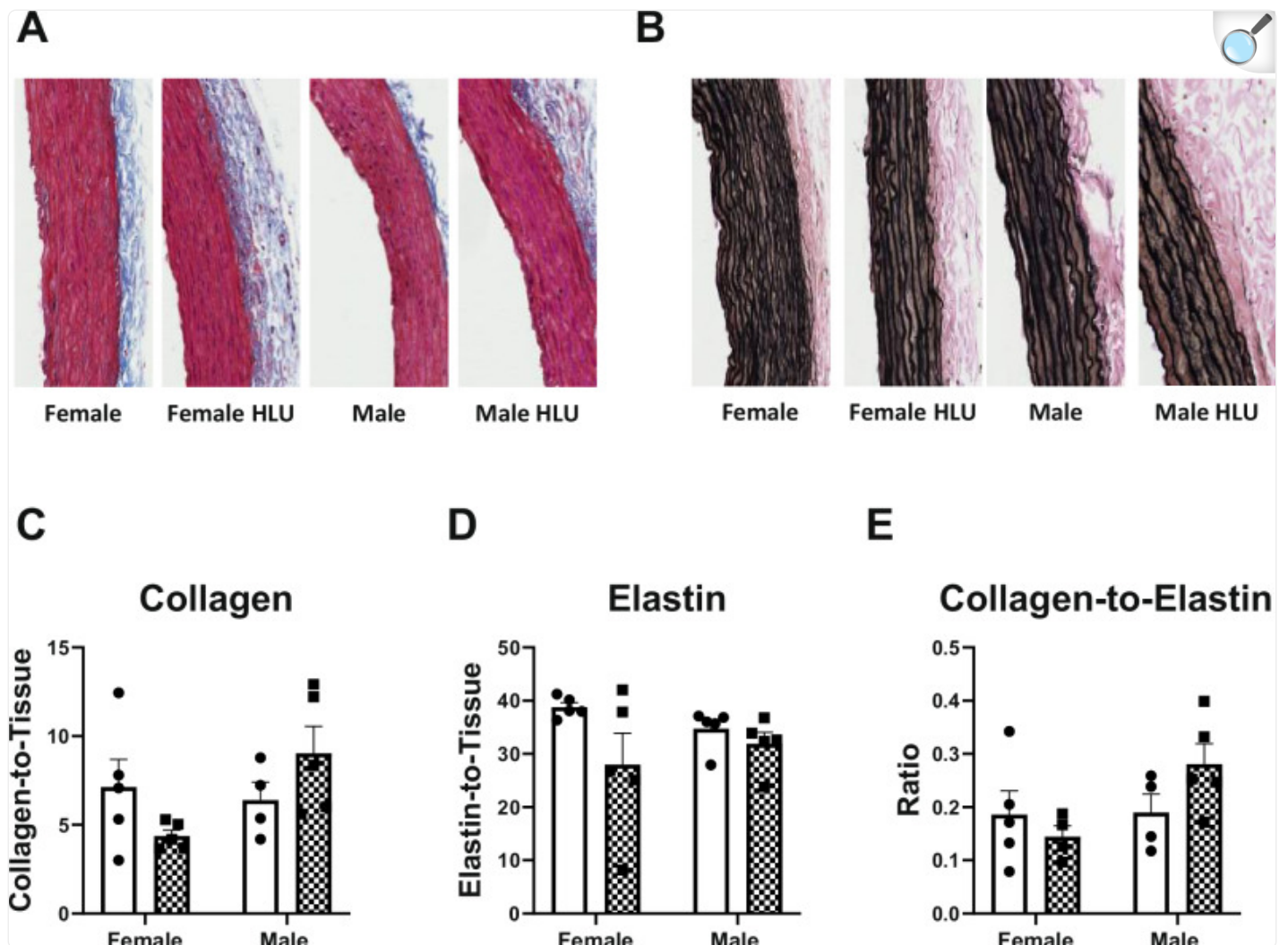
Aortas were stained for collagen by Picrosirius Red stain (**A**, **C**) and elastin by Verhoeff's stain (**B**, **D**). Collagen-to-elastin ratio is shown on panel **E**. Data are mean ± SEM, $n = 4$–5. Magnification: ×20.

Collagen bundling in the aorta was measured by hue analysis to gain understanding of the changes in collagen density after HLU and between sexes (Fig. 5). Results were normalized to the number of total pixels. Through picrosirius red staining and imaging with polarized light, highly dense collagen appears red while very loosely bundled collagen appears green, with orange and yellow colors representing intermediary values (Fig. 5). Hue analysis determined collagen content based on standardized binning of colors as previously reported[15,16]. All groups followed a similar

collagen bundling pattern where prevalence of dense fibers was the highest while the prevalence of fibers with loose collagen was the lowest (Fig. 5). Female control rats had greater red collagen compared with male controls (Fig. 5). However, HLU exposure did not influence the dense collagen fibers (red) in female rats in comparison to control females. Less bundled collagen (yellow and green) was lower in female controls compared to male controls (Fig. 5). HLU did not affect the prevalence of the loosely bundled collagen (yellow or green) in any of the groups. When the data were not normalized to total pixels, female HLU rats had significantly a higher amount of highly dense collagen bundling (red) compared to all other groups (Fig. S3).

Fig. 5. Collagen fiber bundling in the aorta of female and male SD rats in response to HLU.
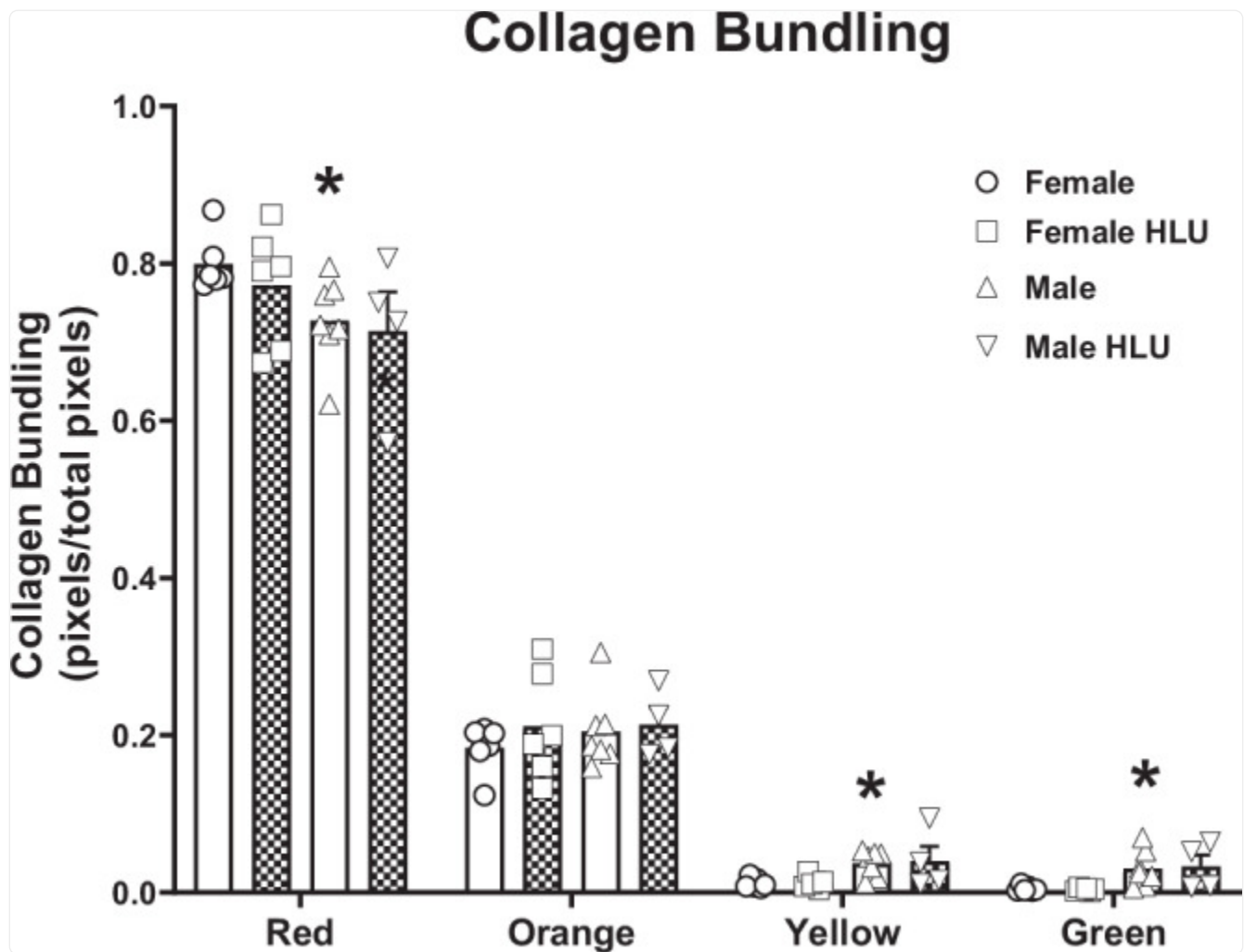
Clear bars indicate control animals; checkered bars indicate rats exposed to hindlimb unloading (HLU). Picrosirius red stained slides were imaged with polarized light, and the pixel values of representative regions were binned into red, orange, yellow, and green hues, corresponding to a respective decrease in collagen bundling. The data are presented as a ratio of the number of pixels of each color category over the total across all color categories per group. Data are mean ± SEM, $n = 4$–7; *$p < 0.05$ versus Control Female.

To determine the alignment of smooth muscle fibers in the aorta, fiber angle was assessed by CurveAlign software. Representative images of the aorta from each group are shown on Fig. 6A. Various additional ECM characteristics such

as fiber straightness, length, and width were analyzed per animal in each group using CT-Fire software. HLU did not affect any of the studied parameters in either male or female groups (Fig. 6B). No differences were evident between sexes in control or HLU-treated groups (Fig. 6B).

Fig. 6. Collagen fiber characterization in female and male SD rats.
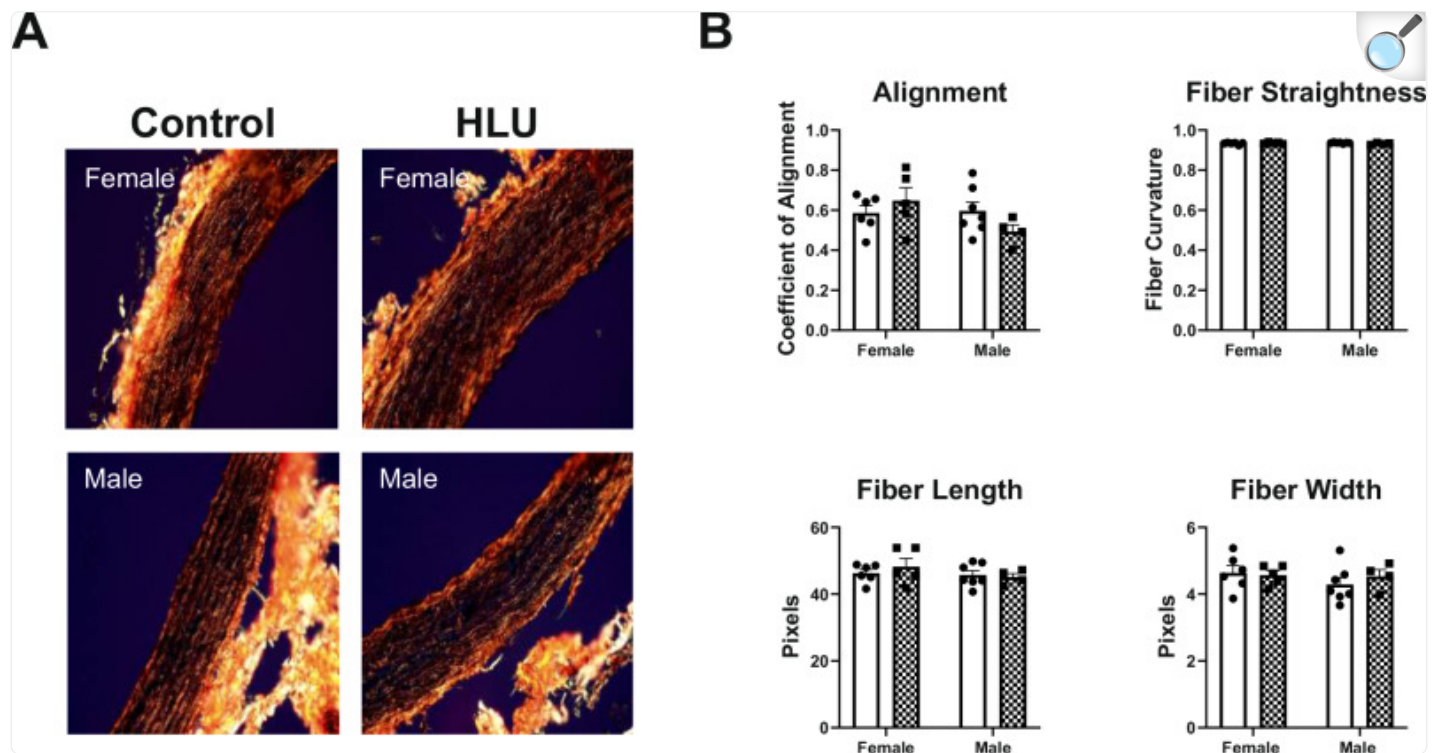
Female and male rat aortas in both control and HLU groups were collected after 14 days of either control or HLU exposure. Picrosirius red stained slides were imaged with polarized light, with representative images from each group shown (**A**). ECM characteristics were analyzed using CT-FIRE software to assess the straightness, length, and width of individual fibers (**B**), with $n = 4$–7 animals per group. Fiber alignment was quantified using CurveAlign software (**B**). Magnification: ×20.

The impact of HLU on aortic GPER

GPER staining in aortic media was lower in control males versus control females. HLU reduced the levels of GPER in females versus control females. No differences in aortic GPER were found in males in response to HLU (Fig. 7).

Fig. 7. GPER levels in female and male SD rats in response to HLU.
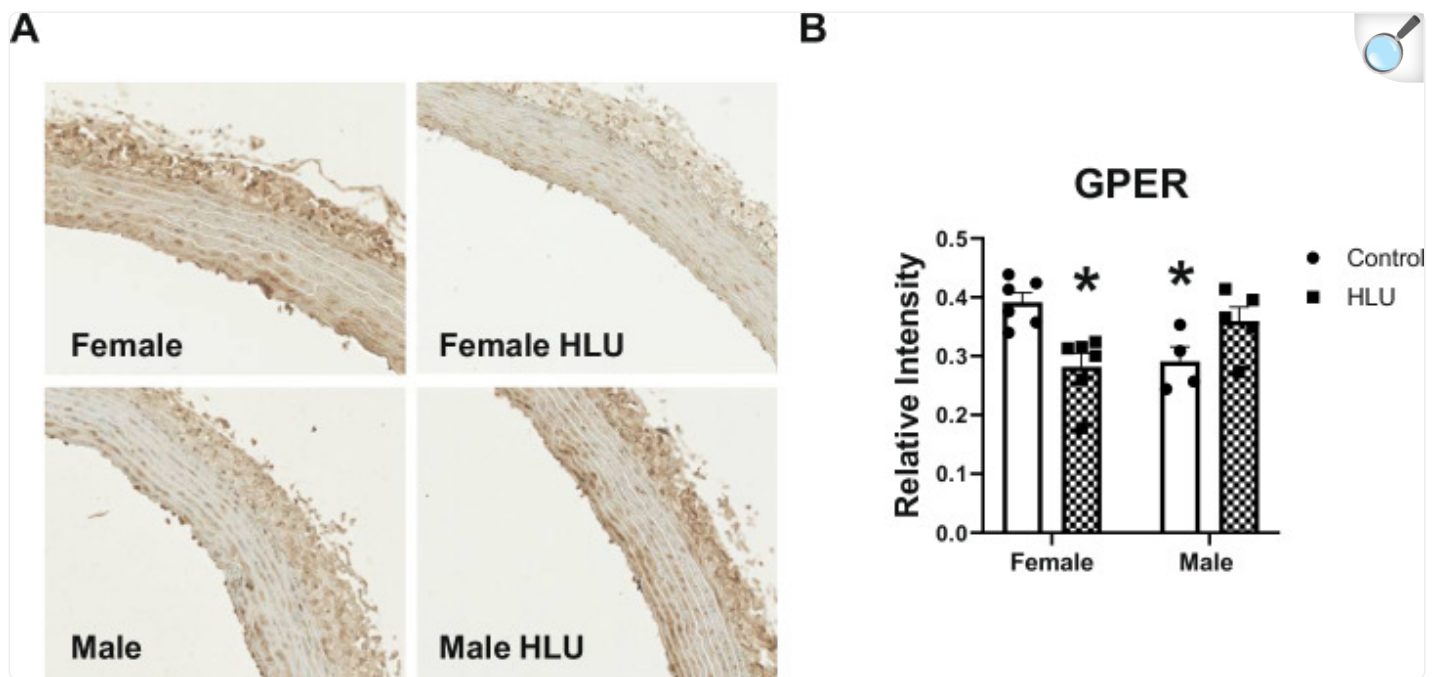
Clear bars indicate control unexposed animals; checkered bars indicate rats exposed to hindlimb unloading (HLU). Representative images of GPER immunostaining (**A**) and data analysis (**B**) are shown. Data are mean ± SEM, *$p < 0.05$ versus Control Female, $n = 4$–6. Magnification: ×20.

The impact of HLU on aortic inflammation, oxidative stress

Male control rats had lower levels of PPAR-γ and COX-2 in the aortic media compared with control female rats (Fig. 8A, B). PPAR-γ levels decreased in female rats following HLU (Fig. 8A). HLU did not affect the levels of COX-2, eNOS, or CD68 in the aortic media of female or male rats (Fig. 8B–D). However, p47 phox and 8-OHdG levels were increased in the aortic media in the female group after HLU compared with the female control group (Fig. 8E, F). 4-HNE was lower in control males versus control females, but no differences were found in the aortas of HLU-exposed females or males versus respective controls (Fig. 8G).

Fig. 8. Aortic injury-relevant markers in female and male SD rats in response to HLU.

A

PPAR γ

Relative Intensity

0.5
0.4 *
0.3 *
0.2
0.1
0.0

Female   Male

B

COX-2

Relative Intensity

0.5
0.4
0.3 *
0.2
0.1
0.0

Female   Male

C

eNOS

Relative Intensity

0.8
0.6
0.4
0.2
0.0

Female   Male

D

CD68

Relative Intensity

0.4
0.3
0.2
0.1
0.0

Female   Male

E

p47 phox

Relative Intensity

0.5
0.4 *   #
0.3
0.2
0.1
0.0

Female   Male

F

8-OHdG

Relative Intensity

0.5
0.4 *
0.3
0.2
0.1
0.0

Female   Male

G

4-HNE

sity

0.5
0.4
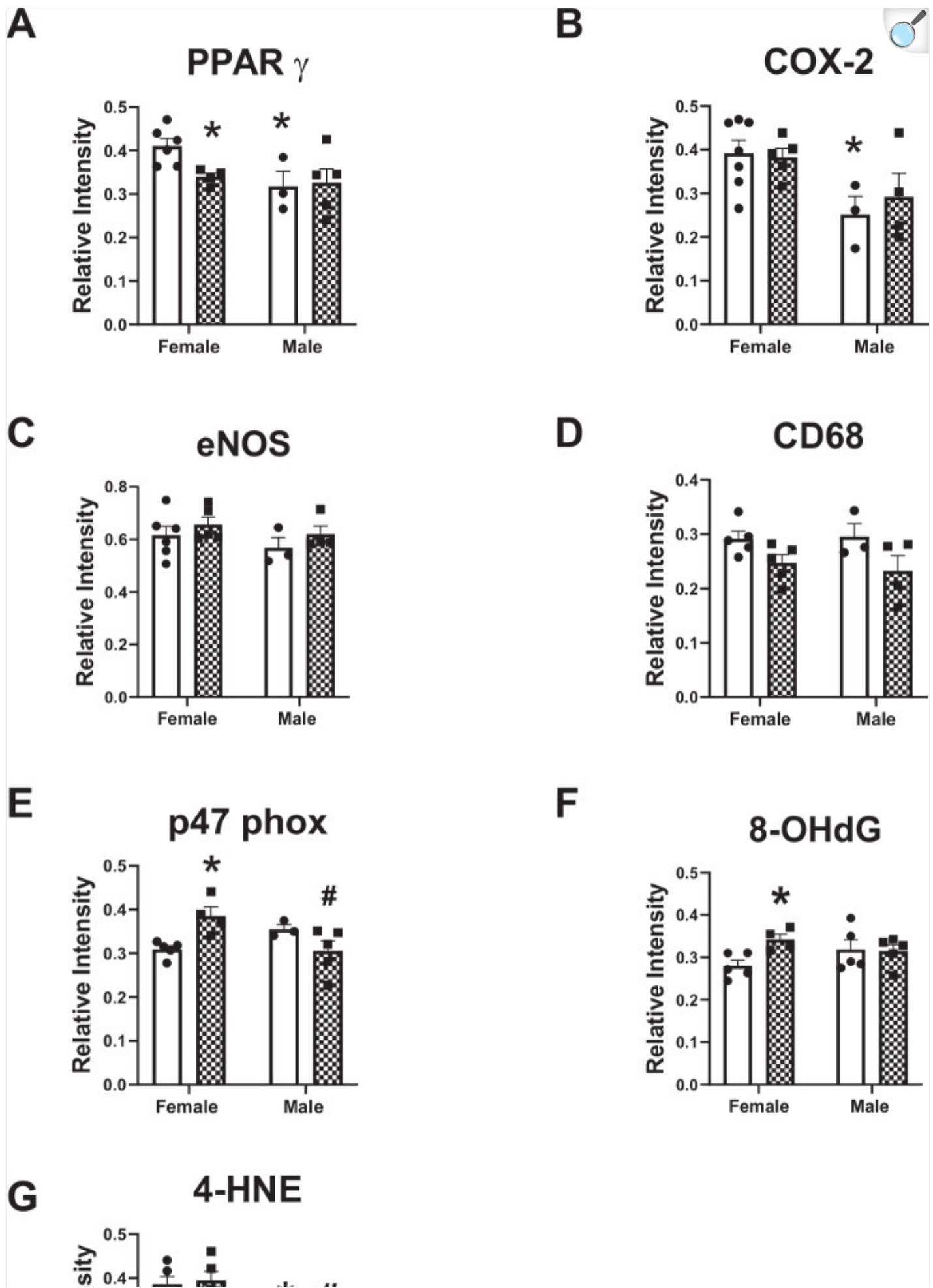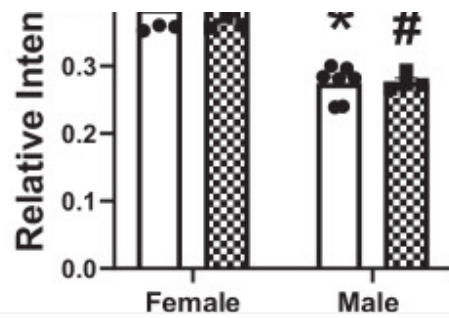
The analysis of immunostaining for various markers relevant for aortic injury is shown (**A–G**). Data are mean ± SEM, *$p < 0.05$ versus Control Female; #$p < 0.05$ versus HLU Female.

G1 effects on aortic PWV, injury markers, uterine weight

There were no differences in body weight or organ weights in G1 treated female SD rats versus control SD females (Table 1). G1 administration reduced aortic arch PWV in female rats exposed to HLU (Fig. 9A). No difference in heart rate was evident in female rats after G1 treatment (Fig. 9B). The levels of 8-OHdG decreased following G1 treatment in HLU female rats (Fig. 9C). No differences in p47phox or PPAR γ levels were detected in HLU females after G1 treatment (Fig. 9D, E).

Table 1.

Characteristics of HLU SD female rats following G1 infusion

	F HLU	F HLU G1
Body weight, g	313.5 ± 12.35	278.5 ± 13.19
Heart weight-to-TL	0.245 ± 0.01	0.213 ± 0.004
Kidney-to-TL	0.308 ± 0.03	0.281 ± 0.02
Pancreas-to-TL	0.234 ± 0.01	0.187 ± 0.01
Spleen-to-TL	0.119 ± 0.006	0.150 ± 0.02
Uterus-to-TL	0.120 ± 0.04	0.125 ± 0.02

Open in a new tab

Data are mean ± SEM, $n = 4$ in each group.

TL tibia length, *g* gram.

Fig. 9. The response to GPER agonist in the female SD rats following HLU.
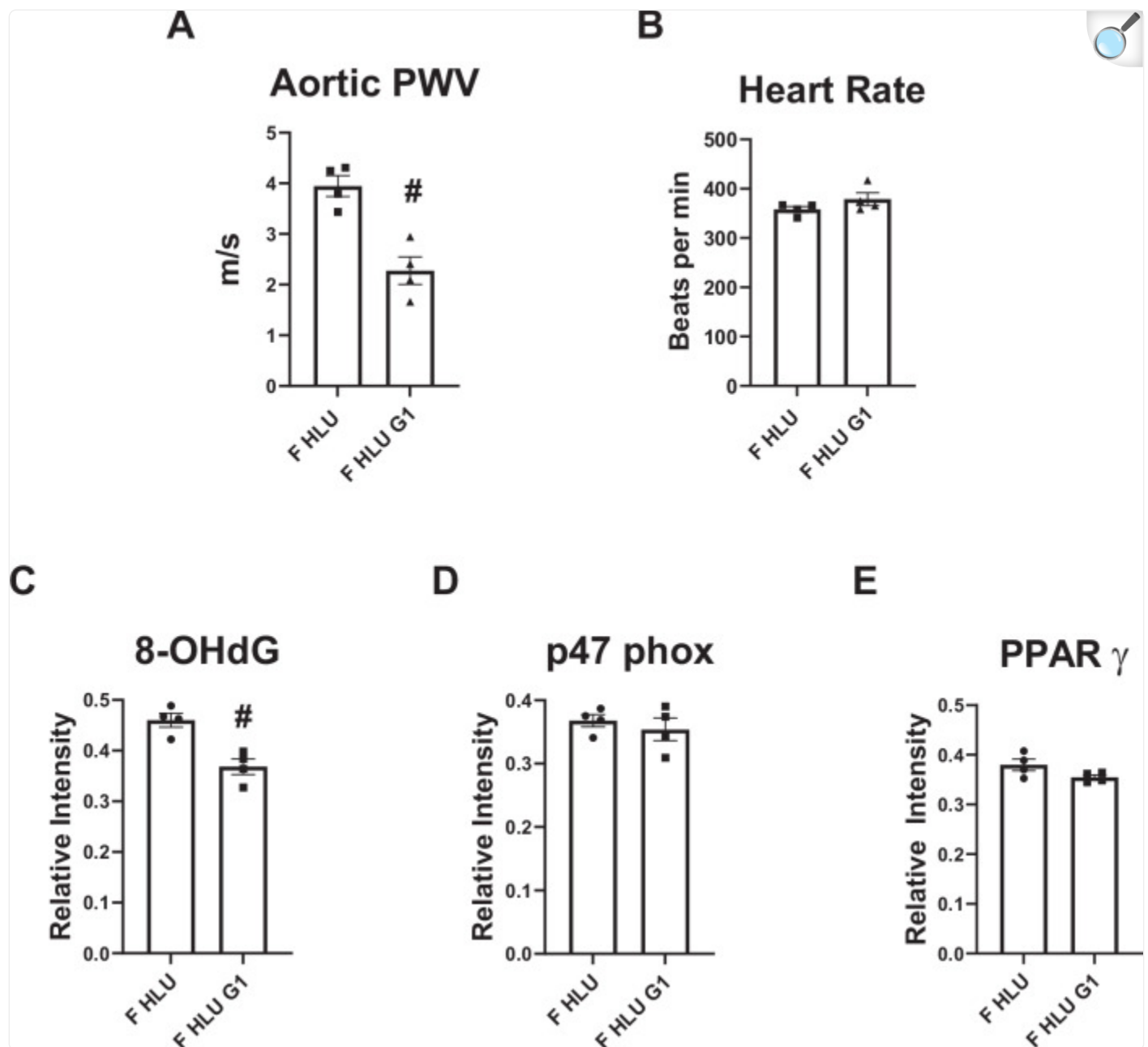
The analysis of aortic arch PWV (**A**), heart rate (**B**), and aortic immunostaining for the markers of oxidative stress and inflammation (**C–E**) are shown. Data are mean ± SEM, [#]$p < 0.05$ versus HLU Female.

Multivariate data analysis

Figure 10 shows graphical representation of DCS analysis of variables depicted in Tables 2 and 3. Table 2 demonstrates differential variable relationships in male versus female SD rats independent of HLU exposure. Several important relationships were identified in males versus females such as oxidative stress markers with ECM characteristics (collagen content and collagen fiber straightness), and arterial stiffness with COX-2 or eNOS. However, in females, the strongest relationships were within body composition parameters; eNOS with lean mass, VSMC actin with elastin, and less strong relationship between GPER with p47phox. These data suggest sex differences in various relationships among variables independent of HLU exposure. Table 3 shows differential variable relationships in control versus HLU SD rats independent of sex. The strongest relationships were identified between variables of body composition with arterial stiffness or with oxidative stress in unexposed control rats. Independent of sex, PPARγ was related to VSMC actin in unexposed controls. In the HLU group, PPARγ was related to collagen; while arterial stiffness - to body composition variables.

Fig. 10. Graphical representation of discrete correlate summation (DCS) analysis of data.
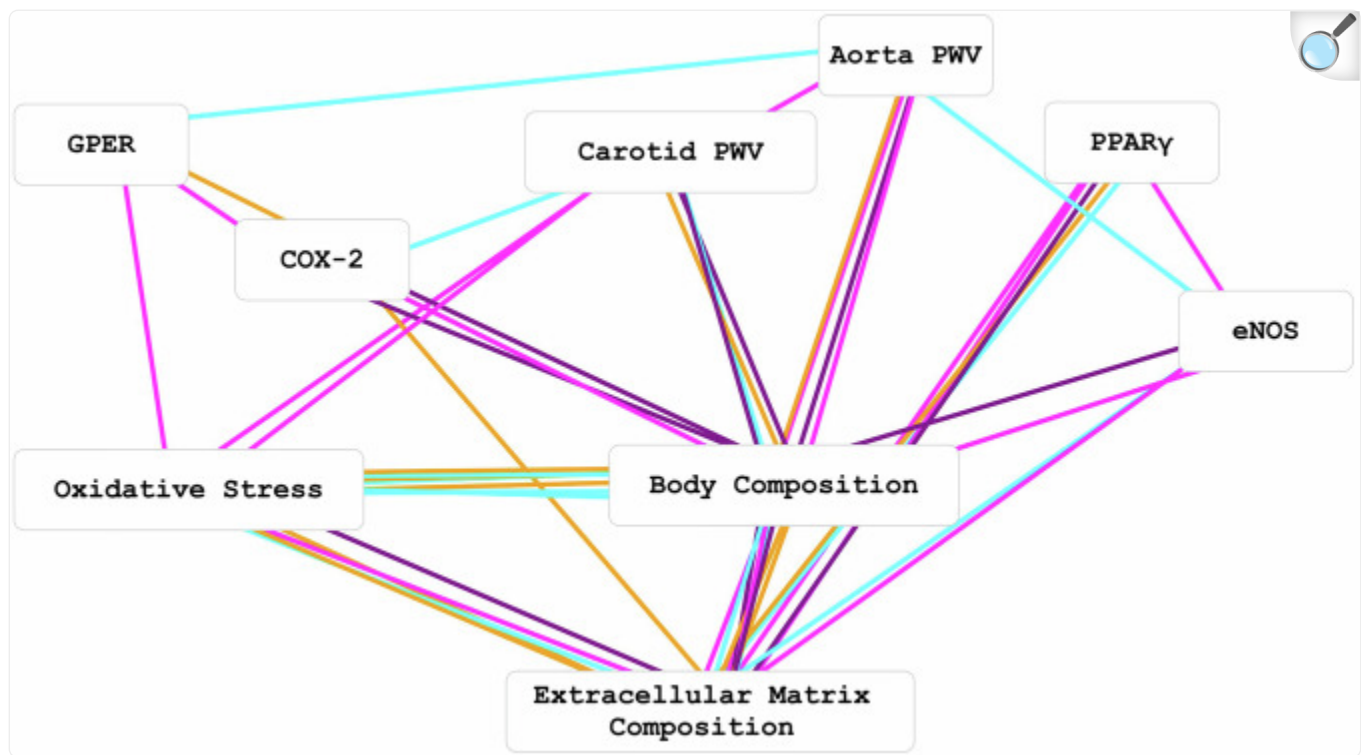
8-OHdG and p47phox were combined into an oxidative stress node[#] (box), VSMC actin, TC, VVG, CF length and CF straightness were combined into an extracellular matrix composition node[#] and Heart/TL, Kidney/TL, BW, % Fat AVE and % Lean mass AVE were combined into a body composition node[#]. Edge (line) colors represent the log correlation ratios of male (cyan) versus female (magenta) [for control and HLU groups, $\log(\text{male}_p/\text{female}_p)$] and the log correlation ratios of HLU (purple) versus control (orange) [for female and male groups, $\log(\text{HLU}_p/\text{control}_p)$]. [#]Multi-feature nodes can have many edges with single feature nodes.

Table 2.

Differential variable relationships in male versus female SD rats independent of HLU exposure

Node 1	Node 2	FC	$\log_{cr}$	Female$_p$	Male$_p$
Heart/TL	Kidney/TL	1840.90	-3.27	0.58874	0.00032
Carotid PWV	COX-2	487.54	-2.69	0.67318	0.00138
Heart/TL	BW	411.90	-2.61	0.18711	0.00045
BW	8-OHdG	216.10	-2.33	0.89683	0.00415
% Fat AVE	% Lean mass AVE	72.03	1.86	0.00634	0.45653
Heart/TL	CF straightness	66.62	-1.82	0.77673	0.01166
CF straightness	p47phox	49.71	-1.70	0.52086	0.01048
Kidney/TL	% Fat AVE	37.06	1.57	0.01487	0.55128
Heart/TL	% Fat AVE	34.88	1.54	0.02029	0.70768
GPER	Aorta PWV	22.80	-1.36	0.20733	0.00909
BW	% Fat AVE	21.68	1.34	0.01406	0.30478
eNOS	TC	21.15	-1.33	0.93269	0.04410
CF straightness	eNOS	19.83	1.30	0.03062	0.60705
BW	% Lean mass AVE	19.40	-1.29	0.01667	0.00086
BW	Kidney/TL	19.27	-1.28	0.00904	0.00047
% Lean mass AVE	eNOS	18.65	1.27	0.02089	0.38976
Kidney/TL	8-OHdG	15.66	-1.19	0.30526	0.01949
Carotid PWV	p47phox	13.74	1.14	0.06155	0.84539
Heart/TL	Aorta PWV	12.96	1.11	0.06002	0.77812
TC	p47phox	12.31	1.09	0.08056	0.99157
BW	TC	12.19	1.09	0.07404	0.90228
CF straightness	PPARγ	10.53	1.02	0.07309	0.76964
Carotid PWV	Aorta PWV	10.52	1.02	0.06299	0.66275
PPARγ	CF length	10.01	-1.00	0.62400	0.06233
8-OHdG	% Lean mass AVE	9.82	-0.99	0.71116	0.07243
eNOS	PPARγ	9.81	0.99	0.08086	0.79300
8-OHdG	Carotid PWV	9.66	0.99	0.10094	0.97512
Heart/TL	TC	9.37	0.97	0.07880	0.73851
VVG	VSMC actin	9.21	0.96	0.04028	0.37113
% Fat AVE	CF straightness	9.05	0.96	0.09821	0.88848
PPARγ	VVG	8.32	0.92	0.08112	0.67508
% Fat AVE	Carotid PWV	8.27	-0.92	0.94384	0.11412
Heart/TL	COX-2	7.73	0.89	0.12050	0.93178
eNOS	Aorta PWV	7.73	-0.89	0.92008	0.11905
% Fat AVE	Aorta PWV	7.72	0.89	0.12160	0.93905
Heart/TL	8-OHdG	7.55	-0.88	0.42922	0.05688

p-value	
< 0.001	
< 0.01	
< 0.05	

% Fat AVE	VSMC actin	6.64	-0.82	0.38153	0.05746
CF straightness	CF length	6.53	0.82	0.09664	0.63121
GPER	p47phox	6.49	0.81	0.02584	0.16763
GPER	COX-2	6.48	0.81	0.14171	0.91868
8-OHdG	p47phox	6.44	0.81	0.10278	0.66142
Kidney/TL	% Lean mass AVE	6.32	0.80	0.01639	0.10362

Log correlation ratios of male (cyan) versus female (magenta); p values: blue $p \leq 0.05$, yellow $p \leq 0.01$, red $p \leq 0.001$.

FC fold change.

Table 3.

Differential variable relationships in control versus HLU SD rats independent of sex

node 1	node 2	FC	log$_{cr}$	control$_p$	HLU$_p$
BW	Kidney/TL	26563.55	4.42	0.00001	0.19333
Heart/TL	Kidney/TL	115.17	2.06	0.00335	0.38627
BW	8-OHdG	80.89	1.91	0.00373	0.30204
Heart/TL	CF straightness	64.10	1.81	0.01511	0.96864
VSMC actin	COX-2	62.94	1.80	0.01069	0.67282
TC	8-OHdG	56.65	1.75	0.00470	0.26619
eNOS	Kidney/TL	50.74	-1.71	0.14111	0.00278
% Fat AVE	Aorta PWV	41.53	1.62	0.02268	0.94195
% Fat AVE	Carotid PWV	26.49	1.42	0.02834	0.75080
Carotid PWV	% Lean mass AVE	20.60	-1.31	0.83025	0.04030
CF straightness	VSMC actin	20.00	-1.30	0.84752	0.04237
TC	PPARγ	17.79	-1.25	0.68631	0.03858
VSMC actin	Kidney/TL	14.01	-1.15	0.61430	0.04384
CF straightness	Kidney/TL	13.49	-1.13	0.20981	0.01555
CF straightness	% Lean mass AVE	13.19	1.12	0.05206	0.68686
Heart/TL	8-OHdG	11.37	1.06	0.03280	0.37299
COX-2	BW	9.38	-0.97	0.95637	0.10192
CF straightness	p47phox	8.95	-0.95	0.70951	0.07925
Carotid PWV	Heart/TL	8.51	-0.93	0.81071	0.09521
VVG	8-OHdG	8.01	0.90	0.07007	0.56097
Heart/TL	COX-2	7.49	-0.87	0.60878	0.08128
GPER	COX-2	6.86	0.84	0.14018	0.96114
Kidney/TL	8-OHdG	6.77	0.83	0.11028	0.74653
VSMC actin	PPARγ	6.72	0.83	0.04834	0.32472
Heart/TL	BW	6.50	0.81	0.00215	0.01398
Heart/TL	Aorta PWV	6.49	-0.81	0.20286	0.03126

p-value
- < 0.001
- < 0.01
- < 0.05

Log correlation ratios of HLU (purple) versus control (orange); p values: blue $p \le 0.05$, yellow $p \le 0.01$, red $p \le 0.001$.

FC fold change.

Discussion

Recent studies highlighted the incidence of arterial stiffness in astronauts following spaceflight. The exposure of rodents to ground-based analogs of microgravity via HLU also demonstrated development of arterial stiffness. However, few studies investigated sex differences and the potential sex-specific mechanisms leading to arterial stiffness due to microgravity. As space exploration continues to expand with longer and more distant missions, understanding the cardiovascular adaptations in female and male astronauts will be crucial to ensure the long-term health and personalized medical care for astronauts[1]. In this study, we investigated sex-specific effects on the cardiovascular system in a rodent-based model of simulated microgravity via 14 days of exposure to HLU[17]. The major findings of this study are that female and male SD rats respond differently to HLU demonstrating a greater arterial stiffness in females at the end of the exposure compared with males. Increased arterial stiffness was accompanied by lower levels of aortic GPER and PPARγ and increased oxidative stress markers (8-OHdG and p47 phox) in females but not males after HLU. The females also exhibited diastolic dysfunction after HLU (males were not evaluated in this experiment). Furthermore, administration of G1, an agonist for the G protein-coupled estrogen receptor GPER, reversed the HLU-induced increase in PWV in female rats and decreased 8-OHdG, suggesting that lower GPER in the setting of simulated microgravity contributes to arterial stiffening. Our findings also suggest that the SD female rat is a suitable model to study mechanisms underlying the development of arterial stiffness in females in response to simulated microgravity.

It is well known that during spaceflight, the cardiovascular system adapts to the state of microgravity by a variety of changes including redistribution of blood flow with fluid shift towards the upper body and decrease in venous return and resistance[18]. Sex differences were reported in the adaptations of the cardiovascular system to spaceflight, however only a few studies investigated the effects of microgravity on arterial stiffening by including subjects of both sexes, and even fewer have made explicit side-by-side comparisons between male and female subjects[1,5,10,19–24]. A few reports also show conflicting results on whether arterial stiffness is reversible following the exposure to microgravity or HDT bed rest[25,26]. Furthermore, the long-term consequences of the exposure to arterial stiffening are unknown but may influence future abnormal hemodynamic responses to stressors and the risk of developing cardiovascular disease particularly in older females[27–32]. A greater aortic PWV in the female SD rats compared to males after HLU suggests sex differences in the development of central arterial stiffening following the exposure to simulated microgravity in this model. PWV differs between women and men during various stages of life ranging from lower baseline PWV in females versus males pre-puberty, similar brachial-ankle PWV in both sexes during adulthood, and a greater increase in PWV in females after menopause suggesting hormonal influences on PWV[33–35]. Furthermore, women undergoing cardiac stress often experience increased aortic wall thickness compared to men, highlighting a potential increased susceptibility of females to developing arterial stiffness[36]. In contrast to other reports, our study did not find changes in arterial stiffness in male SD rats in response to HLU[23]. The response seen in SD rats may be different from those seen in other rodents.

Furthermore, it has been reported that corticosterone levels are lower in resting male SD rats compared with Wistar rats[37], suggesting strain differences in the activity of hypothalamic-pituitary-adrenal (HPA) axis[38]. Since hormonal regulation of vasculature underlies its response to stress, it is safe to assume that the response of male Wistar rats could be exacerbated by greater resting activities of HPA and corticosterone compared with male SD. Furthermore, the exposure length to HLU, age of rats, and the differences in strain responses to stress may explain the observed discrepancies. In addition, HDT bed rest is used to study the responses of cardiovascular system to spaceflight. Sixty-day exposure to HDT increases blood pressure, reduces arterial compliance, and increases arterial stiffness measured by cardiac MRI during the HDT phase in healthy subjects[26]. Surprisingly, another study using the same study cohort found no differences in brachial-femoral pulse wave velocity, but a tendency for an increase of the aortic cross-sectional area was evident suggesting increased vascular filling[39]. The observed vascular changes returned to baseline during the 4 days of recovery suggesting functional mechanisms underlying arterial stiffening in this cohort[26,39]. Of note, no sex effect was observed in these two studies potentially due to small sample size[26,39]. The timing interval of pulse transition time was also decreased in healthy male subjects after 60 day HDT protocol suggesting arterial stiffening[40]. In contrast, increased aortic stiffening measured by carotid-femoral pulse wave velocity did not completely recover after 1 month of head-down bed rest in healthy men without cardiovascular risk[41]. Since arterial stiffness may increase the risk of future cardiovascular disease, understanding the mechanisms leading to arterial stiffening in response to spaceflight may facilitate the development of countermeasures that can improve the cardiovascular health of astronauts post-flight.

The mechanisms of increased arterial stiffness due to microgravity are not well understood. It has been suggested that arterial stiffness could be a compensatory mechanism necessary to maintain cardiac output in response to orthostatic stress after spaceflight[26]. Although we have not directly measured total peripheral resistance, the increased stiffness in females was associated with maintained cardiac output and stroke volume after HLU. In addition, although there was a significant increase in ejection fraction in females after HLU, the ejection fraction values were within the normal range for rats at this age. The significance of these findings needs further investigation by examining the presence of subclinical left ventricle systolic dysfunction using more advanced features of strain rate imaging[42]. In contrast, we found a significant increase in E/E' ratio in female rats after HLU suggesting diastolic dysfunction. These data are in agreement with recent studies including the Framingham Heart Study that reported correlations of arterial stiffness with left ventricular diastolic function[43–45]. It is possible that increased aortic stiffness leads to left ventricular hypertrophy followed by lower filling pressure and reduced coronary flow[45]. Thus, the increased E/E' ratio in females after HLU in addition to greater left common carotid artery stiffness in our study may indirectly suggest the reduction of left ventricle filling pressure. Arterial stiffness, pulse pressure amplification, and augmentation index were greater in women versus men in the Cardiovascular Abnormalities and Brain Lesions study, where the authors suggested that higher arterial stiffness may contribute to higher susceptibility of women to develop heart failure with normal ejection fraction[46]. The return of cardiovascular system to normal functioning after spaceflight may be delayed by lower vasoconstriction of peripheral arteries in those who developed arterial stiffness emphasizing the need for longitudinal assessment of sex-specific risk of cardiovascular events in astronauts with arterial stiffness following long-term spaceflights[47,48]. In addition, other hemodynamic variables such as blood pressure can influence the extent of arterial stiffness. Higher blood

pressures were reported in male SD or male Wistar rats compared to controls after 14 days of HLU[49,50]. Therefore, it is possible that the response of blood pressure after HLU was different in male versus female SD rats contributing to differences in PWV. Our future studies will incorporate blood pressure measurements during HLU exposure to establish the interactions of estrogen receptors and arterial hemodynamics.

Changes in mechanical forces (shear stress and pressure) or ECM composition are important for the regulation of aortic vascular smooth muscle cell (VSMC) support of the arterial compliance and the response of VSMC to increases in blood volume or pressure[51]. We investigated the alterations in ECM components as a potential contributor to increased PWV. Male rats had greater expression of aortic α smooth muscle actin and myosin, however no differences in these cytoskeletal elements were detected in either female or male rats after HLU. In contrast, lower expression of α smooth muscle actin with potential switch to synthetic phenotype was reported in cerebral arteries suggesting vessel-specific alterations in cytoskeleton in response to HLU[52].

An increase in collagen cross-linking and deposition and decrease in elastin content may also lead to increased aortic stiffness and lower arterial compliance. Our findings reveal no differences in collagen content after 14 days of HLU. These data are consistent with reports demonstrating that structural remodeling may not be the primary mechanism leading to arterial stiffness in astronauts after spaceflights[25] suggesting that other factors such as systemic (neurohumoral) or local endothelial factors may have an impact on the development of arterial stiffness[5,23]. However, others reported that HLU resulted in increased deposition of extracellular collagen in the basilar artery but not femoral artery in rats[53]. The hydroxyproline content as a measure of collagen content was increased in male Wistar rats, however collagen subtype composition was not different between control and HLU-exposed rats in this cohort[23]. These studies suggest that hypertrophic response to HLU is vascular bed specific. Furthermore, our data revealed no differences in fiber characteristics including alignment, straightness, length, or width suggesting that 14-day exposure to HLU does not induces changes in collagen fiber characteristics in SD rats. This was a surprising finding considering a possibility of an increased stress on collagen fibers and their potential gradual strengthening under pressure due to HLU[54]. Increased stiffness of collagen fibers may also affect smooth muscle cell phenotype, cell proliferation, or cause downregulation of vascular contractility[55,56]. Increased fiber angle may indicate greater alignment between smooth muscle fibers potentially contributing to increased stiffness[57]. Furthermore, highly dense and stiff matrices can promote crosstalk between estrogen receptors and prolactin supporting the hypothesis that changes of the physical environment, such as in microgravity, can be affected by estrogen receptors[58]. Unlike collagen, another major ECM protein, elastin, is responsible for elasticity, reversible expansion and relaxation of large arteries[59]. Despite elastin being a critical component of the aorta's ability to deform under stress, few studies have investigated elastin in response to HLU exposure. No statistically relevant differences in elastin expression or collagen-to-elastin ratio were found in either female or male rats after HLU exposure. However, the female HLU group had a wide standard deviation which consisted of several subjects having decreased elastin expression after HLU exposure compared to the mean. For those individuals, the cause of decreased elastin after HLU exposure is unclear. Elastin in the aorta could decrease with age or in the setting of arterial stiffness. However, similar to our study, aortic elastin content was not altered in male Wistar rats

after HLU[23].

Sex differences in the cardiovascular system may depend in part on the levels of sex hormone receptors and signaling induced by their actions. In non-pregnant female mice, aortic PWV was reported to be lower in estrus cycle compared with diestrus suggesting that the development of vascular stiffening may in part be influenced by the levels of ovarian hormones[60]. Indeed, our preliminary data agrees with previous reports suggesting that the removal of sex hormones via ovariectomy increases arterial stiffening in the female rats. Furthermore, our preliminary studies show that HLU did not change PWV in aorta or carotid artery of ovariectomized rats (Fig. S4). Similarly, ovariectomy did not exacerbate muscle loss in Fisher female rats during the exposure to either simulated microgravity or partial-gravity environments[61]. These data together with our findings suggest that the activation of local vascular estrogen receptors may have a greater impact on the development of arterial stiffness after HLU than changes in the ovarian hormones. Furthermore, arterial stiffness is associated with genetic variants of estrogen receptor subtypes suggesting a link between arterial stiffness and estrogen receptors expression[62]. Although the data on the status of estrogen receptors in response to spaceflight or microgravity analogs are limited, Holets et al. reported a downregulation of estrogen receptor α mRNA and protein in the uterus and ovary of mice after the spaceflight[63]. However, to our knowledge the response of GPER to HLU in the aorta or other tissues was not yet been considered particularly in the context of sex differences. GPER is a membrane-bound estrogen receptor with protective actions in the cardiovascular system[64]. GPER is widely expressed in tissues throughout the body of both sexes[65]. Our data showed sex differences in aortic GPER levels between unexposed animals. However, this difference was lost when GPER decreased in the females after HLU. In addition, our data revealed a strong relationship between aortic pulse-wave velocity and GPER in males. In agreement with previous reports, G1 administration reduced aortic pulse-wave velocity demonstrating a protective role of GPER activation against arterial stiffening[66–71]. Recent preclinical studies highlighted a protective role of GPER in the regulation of blood pressure, diastolic function, vascular reactivity, arterial stiffness, and aortic remodeling[66–71]. In contrast, the knockout of GPER in male mice increased endothelial prostanoid-mediated vasoconstriction of the thoracic aorta without changing eNOS mRNA levels or eNOS activity[72]. In addition, the intracarotid pulse wave velocities were similar between male and female GPER knockout mice, however the response to angiotensin II showed greater increases in elastin and smooth muscle but less collagen deposition in male GPER knockout mice versus females revealing sex differences in vascular remodeling[67].

Aortic pulse-wave velocity in HLU males was also correlated with heart weight. Indeed, heart weight was lower in male SD after HLU, but did not change in females. The mechanisms and consequences of reduced heart weight in SD HLU male rats are unknown, while cardiac atrophy was suggested to contribute to the reductions in cardiac function after spaceflight[18]. Furthermore, although estrogen has an established role in the regulation of adiposity, the effect of GPER deletion on body weight revealed contrasting results with studies reporting increased or decreased body weight in GPER knockout mice versus control counterparts[73,74]. Our data showed no changes in body weight, fat mass or lean mass in females after HLU, however similar to other reports, HLU decreased lean body mass in male SD rats[75]. In addition, there was strong correlation between body weight and lean body mass in both sexes. These changes appeared to be

unrelated to GPER as no relationship between lean mass and GPER was detected. Fat mass however was not different among studied groups potentially due to small number of subjects used for this analysis which led to large data variability in female controls and male subjects. Future studies using GPER knockout mice of both sexes could provide more insight on the role of GPER in vascular adaptations to HLU.

Since GPER actions has been linked to antioxidant effects in cardiovascular system[65,76], we tested the levels of oxidative stress markers in the aorta of female versus male rats following HLU. Our data showed increased levels of DNA damage marker 8-OHdG in the aorta of HLU females but not in male rats suggesting increased oxidative stress. Furthermore, the absence of differences in the levels of lipid peroxidation marker 4-HNE suggests a more pronounced DNA damage[77]. In agreement, a 72-h exposure to simulated microgravity through a rotary cell culture system resulted in increased expression of the DNA damage markers in human promyelocytic leukemia cells[78]. Previous reports also demonstrated increased circulating levels of 8-OHdG in rats after HLU, in human patients with cardiovascular disease, as well as in patients with diabetes where higher 8-OHdG was positively correlated with PWV[79–81]. Lower levels of antioxidant enzymes catalase and glutathione peroxidase were reported in skeletal muscle of male SD rats after 28 days of HLU suggesting that lower activity of antioxidant enzymes may also contribute to the increase of superoxide levels after HLU[82]. The correlations of 8-OHdG with collagen and to a lesser degree with elastin in our study suggest that long-term exposure to oxidative stress could promote ECM remodeling and further exacerbate aortic stiffening in response to HLU[83]. Furthermore, the reduction of pulse wave velocity by G1 administration in HLU females was accompanied by decreased 8-OHdG suggesting that the protective actions of GPER may involve reduction of vascular oxidative stress[70]. These data agree with previous reports demonstrating antioxidant effects of GPER activation in various tissues including aorta of hypertensive rats where 2-week administration of G1 reduced lipid peroxidation[68]. Although the major strength of our studies was a comparison between female and male SD rat responses to HLU, G1 treatment experiments were performed only in female rats, thus sex specific responses to G1 were not established; thus, future studies should also consider the response of male SD subjects to G1 activation in the setting of HLU.

A crosstalk between GPER and PPARγ in anti-inflammatory protection against global cerebral ischemia has been suggested in ovariectomized rats[84]. PPARγ is a member of the nuclear receptor superfamily involved in estrogen-based protection of the cardiovascular and renal systems[85,86]. PPARγ is also closely linked to cardiovascular and metabolic dysfunction and therefore has the potential for being targeted by HLU which induces cardiovascular changes similar to aging or menopause[87]. Our data revealed lower PPARγ levels in the aorta of female rats in response to HLU[88], as well as a correlation of PPARγ with collagen content in HLU aortas. Considering the role of PPARγ in the regulation of vasodilation, vascular redox state, bioavailability of nitric oxide, as well as regulation of VSMC stiffness[89], our data implies that lower PPARγ may result in reduced protection against arterial stiffness caused by the exposure to HLU. Indeed, the activation of PPARγ by pioglitazone attenuated arterial stiffness and obesity-induced elastin fiber fragmentation in perivascular adipose tissue of diabetic mice suggesting that protective effects of PPARγ against arterial stiffening may involve ECM remodeling mechanisms[90]. Furthermore, we investigated the expression patterns of CD68-positive macrophage/monocytes, eNOS and COX-2 in the aorta after HLU. The eNOS regulation in the vasculature in

response to HLU may depend on the vascular bed or the length of the exposure[47,91]. Lower nitric oxide availability due to formation of peroxynitrite has been suggested as a contributing factor to superoxide production in vasculature after HLU[92]. However, our data revealed no differences in eNOS or COX-2 among studied groups. Future studies will assess nitric oxide bioavailability and aortic vascular reactivity in response to nitric oxide and COX-2 inhibition to determine if functional vasodilatory responses are altered in female rats after HLU. Although no differences in eNOS levels were detected in male aortas, there was a strong correlation between eNOS and ECM in male SD suggesting a potential influence of eNOS on ECM remodeling. However, a small sample size in the analysis of immunostaining of various vascular markers or G1 treatment potentially limited our ability to detect significant effects between study groups. The use of multivariate analysis of data provided additional insights on potential relationships between studied variables; thus, strengthening the conclusions of this study.

Finally, the mechanisms and long-term consequences of arterial stiffness developed in response to spaceflight are not well understood. The present study demonstrated sex differences in the development of arterial stiffening in SD rats exposed to simulated microgravity. Although the cellular mechanisms of the interaction between microgravity, the cardiovascular system and estrogen receptors in response to HLU need further investigation, our study revealed that lower GPER in the females contributes to the development of arterial stiffness during HLU, and that the SD rat is a suitable model to study these interactions. Furthermore, multivariate statistical analysis identified several significant relationships between studied variables based on sex or the exposure to HLU that could be explored in future studies focused on the development of destiffening agents as a countermeasure for arterial stiffness.

Methods

Animals

The study was approved by the Institutional Animal Care and Use Committee of the Wake Forest University School of Medicine (A21-039). Female and male Sprague-Dawley (SD) rats were purchased from Charles River Laboratories (Wilmington, MA, USA). All rats were housed at 12:12-h light-dark cycle, a constant room temperature and humidity. A standard rodent chow (Lab Diet 5P00 - Prolab RMH 3000, PMI Nutrition International, INC, Brentwood, MO) and water were given ad libitum throughout the experimental protocols.

Study timeline

Socially and sexually mature female and male SD rats at 20 weeks of age were randomly assigned to study groups. The first experimental set included the following animals: female control (F), female HLU (F HLU), male control (M), or male HLU (M HLU) ($n = 5$–8 in each group). HLU groups underwent hindlimb unloading for 14 days[93]. Control groups were exposed to the same cages for a 14-day period. On the morning of day 14, animals were imaged with ultrasound

followed by EchoMRI, and then sacrificed to collect tissues. Additional experimental set included two groups of HLU female rats that underwent either treatment with G1, a G protein-coupled estrogen receptor (GPER) agonist (Cayman Chemical, Ann Arbor, MI) or vehicle ($n = 4$ in each group). G1 was dissolved in 50% dimethylsulfoxide (DMSO) at a dose of 100 µg/kg/day. G1 or vehicle was delivered via osmotic minipumps to female HLU rats for 3 weeks (model 2ML2; Alza Corp., Palo Alto, CA)[94]. Pumps were implanted subcutaneously on the back of the rat's neck 1-week prior to HLU exposure and continued for 2 weeks during the HLU exposure. Aortic pulse wave velocity (PWV) and injury markers were analyzed at the end of the 3-week treatment with G1.

Hindlimb unloading (HLU)

To determine the effects of microgravity, 20-week-old male and female SD rats were suspended by the tail via HLU for 14 days resulting in a head-down body angle of 30–35 degrees. Age-matched, non-suspended controls remained in similar cages[93]. Animals were monitored for signs of distress by monitoring food and water intake and loss of body weight throughout the exposure to HLU.

Ultrasound assessment of arterial stiffness

Rats were anesthetized with isoflurane (1.5%) and placed on a temperature-controlled platform. Electrocardiogram (ECG) and heart rate were monitored throughout the imaging protocol. Hair was removed from the thoracic and neck areas of rats with a depilatory cream prior to imaging. Pulse wave velocity (PWV) of the aortic arch and common carotid arteries were determined in male and female rats using a MS250 transducer and high-resolution ultrasound imaging system Vevo 2100 LAZR (FujiFilm, VisualSonics). MS250 transducer operates at a frequency of 13–24 MHz and axial resolution of 75/165. The PWV of the aortic arch and carotid arteries was measured by the following equation: the D (mm), distance from ascending to descending artery measured with tracing tool (Vevo Lab software), divided by time interval, Δt, which represent the difference between $t2$ and $t1$ (ms). Time intervals between the R-wave of the ECG to the foot of the Doppler waveforms were averaged over at least three cardiac cycles. The foot of the Doppler waveform was defined manually as the intersection between the baseline and the beginning of the ascending or descending aortic velocity, or proximal and distal segments of the common carotid artery. The pulse-transit time in the aortic arch was calculated by subtracting the mean ascending aorta ($t1$) time interval from the mean descending aorta ($t2$) time interval. For common carotid arteries, $t1$ time interval was recorded from the proximal portion of the artery and $t2$ time interval was recorded from distal portion of the artery. All ultrasound measurements were done by one operator, blinded to the experimental groups.

Ultrasound assessment of diastolic function

Left ventricle M-mode images were recorded in the short-axis parasternal view. The ejection fraction (EF) was

calculated as %EF = ((left ventricle end-diastolic volume (LVEDV) − left ventricular end-systolic volume (LVESV)/ LVEDV) × 100. Stroke volume (SV) was determined as SV = (LVEDV − LVESV) µl. Cardiac output (CO) was determined as cardiac output (CO) = heart rate (HR) × SV/1000 ml/min. Mitral inflow measurements of early- (E_{max}) and late (A_{max}) filling velocities were acquired from an apical four-chamber heart orientation using pulsed wave Doppler with the sample volume placed at the tips of mitral leaflets. The mitral valve septal annular velocities (E′) were also assessed by Doppler tissue imaging from the four-chamber view[69]. A ratio of E/E' was computed as a measure of left ventricular end-diastolic pressure. Greater E/E' suggests higher left ventricular end-diastolic pressure. All measured and calculated systolic and diastolic indices are represented as the average of at least three consecutive cardiac cycles.

Body composition

EchoMRI^{TM} Analyzer was used to determine the total body composition in studied groups. Briefly, animal was placed in a clear holder, and then inserted into the EchoMRI Analyzer without anesthesia. Each animal was scanned three times in a row and the average total body fat and lean mass were recorded.

Collagen content

Aortas were fixed in formalin and ethanol followed by the paraffin-embedding. Aortic sections were cut at thickness of 5 µm. Collagen content was determined by Masson's trichrome staining (Abcam ab150686). Using a Hamamatsu Nanozoomer 2.0 HT equipped with NDP.scan and NDP.view, slides containing stained aortic sections were imaged at ×20 magnification. Using Adobe Photoshop 7.0, each slide was quantified for the total area of collagen deposition (red, orange, yellow, or green) and reported as a collagen-to-tissue ratio.

Collagen fiber properties

Five µm sections were stained with Picrosirius red (Sigma-Aldrich, St. Louis, MO; assay components Cat#: 197378-100G; P6744-16A; 36-554-8) to assess collagen fiber properties. Slides were imaged using polarized light, and 90 × 90 µm representative regions of interest (ROIs) were selected around aortic arch to determine collagen fiber bundling, length, width, straightness, and alignment. Collagen bundling was assessed using an R script that binned hue values in each ROI into red, orange, yellow, and green, in order of high to low collagen bundling[15]. Data was presented as a ratio of the binned values to the total number of pixels binned.

Collagen fiber length, width, and straightness were determined through CT-FIRE software (Laboratory for Optical and Computational Instrumentation, The University of Wisconsin-Madison) using default settings[95]. Coefficient of alignment was determined through CurveAlign software (Laboratory for Optical and Computational Instrumentation, The University of Wisconsin-Madison), using default settings[95].

Smooth muscle fiber characterization

Extracellular matrix (ECM) characteristics were analyzed using MATLAB and the CT-FIRE algorithm to assess fiber straightness, fiber length, and fiber width. Fiber angle was quantified at the individual fiber level. CT-FIRE excludes empty pixels prior to analysis. Quantification of fibers was done using CT-FIRE and Curve Align scripts[15].

Elastin fiber content

Verhoeff's stain (American MasterTech; Cat#: KTVEL) was used to quantify elastin content in aortic sections using the manufacturer's protocol. The staining intensity in the tunica media layer of the aorta was normalized to the intensity of the background and to the maximal value of 255 of the red, green, and blue intensity (RGB) component and reported as relative intensity units[96].

Morphological, inflammatory, and oxidative stress markers

Tissues were fixed in 10% formalin followed by 70% ethanol, embedded in paraffin, and cut into 5 µm sections. Immunostaining was performed using the avidin biotin complex (ABC) method with 0.1% diaminobenzene solution used as the chromogen as previously described. Antigen retrieval treatment with sodium citrate buffer (pH 6.0) was applied at 90–95 °C for 30 min. Non-specific binding was blocked in a buffer containing 10% normal goat serum, 0.1% Triton-X in PBS for 30 min. Aortic sections were incubated with goat anti-α-smooth muscle actin (1:500 dilution; Novus Biologicals, Centennial, CO, USA; Cat#: NB300-978), rabbit anti-smooth muscle myosin heavy chain 11 (1:500 dilution; Abcam, Waltham, MA, USA; Cat#: ab53219), rabbit anti-4-hydroxynonenal (4-HNE; 1:10,000 dilution; Abcam, Waltham, MA, USA; Cat#: ab46545), rabbit anti-p47 phox (1:400 dilution; LifeSpan BioSciences, Shirley, MA, USA; Cat#: LS-C331296), mouse anti-8-hydroxy-2'-deoxyguanosine (8-OHdG; 1:100 dilution; JaICA, Fukuroi, Shizuoka, Japan; Cat#: MOG-020P), rabbit anti-cyclooxygenase-2 (COX-2, 1:200 dilution; Cayman Chemicals, Ann Arbor, MI, USA; Cat#: 160126), mouse anti-endothelial nitric oxide synthase (eNOS, 1:100 dilution; BD Biosciences, Franklin Lakes, NJ; Cat#: 610297), mouse anti-macrophages/monocytes antibody, clone ED-1/CD68 (1:200 dilution; MilliporeSigma, Burlington, MA, USA; Cat#: MAB1435), rabbit anti-peroxisome proliferator-activated receptor gamma (PPARγ; 1:1200 dilution; Biorbyt, LLC, Durham, NC, USA; Cat#: orb11291), rabbit anti-GPER (1:200 dilution; Biorbyt, LLC, Durham, NC, USA; Cat#: orb10740) and secondary biotinylated anti-rabbit, mouse or goat antibodies (1:500 dilution; Vector Laboratories, Burlingame, CA, USA). Slides were scanned with a Hamamatsu Nanozoomer 2.0 HT utilizing NDP.scan and NDP.view as the imaging software at ×20 magnification. Images were analyzed in four fields per aortic cross-section using Adobe Photoshop 7.0 by the investigator blinded to the experimental groups. The staining was normalized to the intensity of the background and to the maximal value of the RGB component and reported as relative intensity units as described[96].

Statistics

Groups were compared using one-way or two-way analysis of variance (ANOVA) followed by the Bonferroni post hoc tests (GraphPad Software, San Diego, CA). A p value <0.05 was considered statistically significantly different. All data were presented as mean ± SEM.

Discrete correlate summation (DCS) analysis

The microgravity and sex discrete correlate summation (DCS) analysis is designed to create an indexed network for the visualization of binary interaction of variables with large differences in sex-wise correlations given this model of microgravitational challenge and a microgravitational-wise correlations independent of sex. DCS analysis was performed on the 18 variables (Heart/TL, Kidney/TL, BW, % Fat AVE, % Lean mass AVE, COX-2, eNOS, GPER, PPARγ, VSMC actin, 8-OHdG, p47phox, TC, VVG, Carotid PWV, Aorta PWV, CF length, CF straightness). Briefly, absolute values of both the log correlation ratios ($\log_{cr}$) of male versus female (for control and HLU groups, $\log(\text{male}_p/\text{female}_p)$) and the log correlation ratios of HLU versus control (for female and male groups, $\log(\text{HLU}_p/\text{control}_p)$) were calculated for each variable combination[97]. To find large differences between the sex-wise and microgravity-wise correlations (153 combinations from each DCS analysis), we performed these analyses to isolate correlations of interest; 68 combinations ($|\log_{cr}| \geq 0.8$) were further evaluated after tabulating and indexing by DCS; $|\log_{cr}|$ values range from 0.8 to 4.42 or 6.3-fold to 27,000-fold change in p values. For network visualization purposes 8-OHdG and p47phox were combined into an oxidative stress node, VSMC actin, TC, VVG, CF length and CF straightness were combined into an extracellular matrix composition node and Heart/TL, Kidney/TL, BW, % Fat AVE and % Lean mass AVE were combined into a body composition node.

The 68 above $|\log_{cr}| \geq 0.8$ edges were plotted with the corresponding variable nodes in Fig. 10. Nodes and edges also illustrated in Tables 2 and 3. All calculations were performed in Excel (Microsoft Corp., WA), Prism (GraphPad Software, MA) was used for statistical analyses and plotting data in figures; Cytoscape was used for network generation.

Supplementary information

Supplementary material (232.4KB, pdf)

Acknowledgements

Abbreviations

SD

Sprague Dawley rat

HLU

Hindlimb unloading

PWV

pulse wave velocity

GPER

G protein-coupled estrogen receptor

PPARγ

peroxisome proliferator-activated receptor γ

8-OHdG

8-hydroxy-2'-deoxyguanosine

SANS

spaceflight associated neuro-ocular syndrome

ROIs

regions of interest

4-HNE

4-hydroxynonenal

COX-2

cyclooxygenase-2

eNOS

endothelial nitric oxide synthase

HPA

hypothalamic-pituitary-adrenal axis

VSMC

vascular smooth muscle cell

ECM

extracellular matrix

Author contributions

Ebrahim Elsangeedy performed the experiments, acquired and interpreted the data; Dina N. Yamaleyeva analyzed and interpreted the data, wrote and revised the manuscript; Nicholas P. Edenhoffer analyzed, and interpreted the data, revised the manuscript; Allyson Deak, Anna Soloshenko, Omar H. Shaltout, and Nildris CruzDiaz acquired, analyzed, and interpreted the data; Jonathan Ray and Xuming Sun performed the experiments, analyzed the data, revised the manuscript; Brian Westwood analyzed and interpreted the data, wrote and revised the manuscript; Daniel Kim-Shapiro, Debra I. Diz, Shay Soker, and Victor M. Pulgar interpreted the data, revised the manuscript; April Ronca consulted on study design and data interpretation, revised the manuscript; Jeffrey S. Willey provided expertise on HLU model and study design; Liliya M. Yamaleyeva conceived and designed the research, analyzed and interpreted the data, wrote and revised the manuscript.

Data availability

The data that support the findings of this study are available in "Methods", "Results", "Discussion" and/or Supplementary Material of this article.

Competing interests

The authors declare no competing interests.

Footnotes

Publisher's note Springer Nature remains neutral with regard to jurisdictional claims in published maps and institutional affiliations.

These authors contributed equally: Ebrahim Elsangeedy, Dina N. Yamaleyeva.

Supplementary information

The online version contains supplementary material available at 10.1038/s41526-024-00450-z.

References

1. Platts, S. H. et al. Effects of sex and gender on adaptation to space: cardiovascular alterations. *J. Womens*

Health **23**, 950–955 (2014). [DOI   ] [PMC free article] [PubMed] [Google Scholar   ]

2. Uri, J. *Women's History Month 2023: Celebrating Women Astronauts* (NASA.gov, 2023).

3. Jirak, P. et al. How spaceflight challenges human cardiovascular health. *Eur. J. Prev. Cardiol.* **29**, 1399–1411 (2022). [DOI   ] [PubMed] [Google Scholar   ]

4. Kunz, H. et al. Alterations in hematologic indices during long-duration spaceflight. *BMC Hematol.* **17**, 12 (2017). [DOI   ] [PMC free article] [PubMed] [Google Scholar   ]

5. Hughson, R. L. et al. Increased postflight carotid artery stiffness and inflight insulin resistance resulting from 6-mo spaceflight in male and female astronauts. *Am. J. Physiol. Heart Circ. Physiol.* **310**, H628–H638 (2016). [DOI   ] [PubMed] [Google Scholar   ]

6. Norsk, P., Asmar, A., Damgaard, M. & Christensen, N. J. Fluid shifts, vasodilatation and ambulatory blood pressure reduction during long duration spaceflight. *J. Physiol.* **593**, 573–584 (2015). [DOI   ] [PMC free article] [PubMed] [Google Scholar   ]

7. Lee, S. M. C. et al. Arterial structure and function during and after long-duration spaceflight. *J. Appl. Physiol.* **129**, 108–123 (2020). [DOI   ] [PubMed] [Google Scholar   ]

8. Willey, J. S. et al. The individual and combined effects of spaceflight radiation and microgravity on biologic systems and functional outcomes. *J. Environ. Sci. Health C Toxicol. Carcinog.* **39**, 129–179 (2021). [DOI   ] [PMC free article] [PubMed] [Google Scholar   ]

9. Mader, T. H. et al. Optic disc edema, globe flattening, choroidal folds, and hyperopic shifts observed in astronauts after long-duration space flight. *Ophthalmology* **118**, 2058–2069 (2011). [DOI   ] [PubMed] [Google Scholar   ]

10. Mark, S. et al. The impact of sex and gender on adaptation to space: executive summary. *J. Womens Health* **23**, 941–947 (2014). [DOI   ] [PMC free article] [PubMed] [Google Scholar   ]

11. Waters, W. W., Ziegler, M. G. & Meck, J. V. Postspaceflight orthostatic hypotension occurs mostly in women and is predicted by low vascular resistance. *J. Appl. Physiol.* **92**, 586–594 (2002). [DOI   ] [PubMed] [Google Scholar   ]

12. Morey, E., Sabelman, E., Turner, R. & Baylink, D. A new rat model simulating some aspects of space flight. *Physiol* **22**, S23–4 (1979). [PubMed] [Google Scholar   ]

13. Hargens, A. R. & Vico, L. Long-duration bed rest as an analog to microgravity. *J. Appl. Physiol.* **120**, 891–903 (2016). [DOI   ] [PubMed] [Google Scholar   ]

14. Yin, F. C., Spurgeon, H. A., Rakusan, K., Weisfeldt, M. L. & Lakatta, E. G. Use of tibial length to quantify cardiac hypertrophy: application in the aging rat. *Am. J. Physiol.* **243**, H941–H947 (1982). [DOI] [PubMed] [Google Scholar]

15. Liu, Y., Keikhosravi, A., Mehta, G. S., Drifka, C. R. & Eliceiri, K. W. Methods for quantifying fibrillar collagen alignment. *Methods Mol. Biol.* **1627**, 429–451 (2017). [DOI] [PMC free article] [PubMed] [Google Scholar]

16. Rich, L. & Whittaker, P. Collagen and picrosirius red staining: a polarized light assessment of fibrillar hue and spatial distribution. *J. Morphol. Sci.* **22** (2005).

17. Hargens, A., Steskal, J., Johansson, C. & Tipton, C. Tissue fluid shift, forelimb loading, and tail tension in tail-suspended rats. *Physiol.* **27**, 37–38 (1984). [Google Scholar]

18. Globus, R. K. & Morey-Holton, E. Hindlimb unloading: rodent analog for microgravity. *J. Appl. Physiol.* **120**, 1196–1206 (2016). [DOI] [PubMed] [Google Scholar]

19. Ronca, A. E. & Alberts, J. R. Physiology of a microgravity environment selected contribution: effects of spaceflight during pregnancy on labor and birth at 1 G. *J. Appl. Physiol.* **89**, 849–854 (2000). [DOI] [PubMed] [Google Scholar]

20. Casey, T. et al. Hypergravity disruption of homeorhetic adaptations to lactation in rat dams include changes in circadian clocks. *Biol. Open* **1**, 570–581 (2012). [DOI] [PMC free article] [PubMed] [Google Scholar]

21. Patel, O. V. et al. Lipogenesis impaired in periparturient rats exposed to altered gravity is independent of prolactin and glucocorticoid secretion. *Eur. J. Appl. Physiol.* **104**, 847–858 (2008). [DOI] [PubMed] [Google Scholar]

22. Plaut, K., Maple, R. L., Wade, C. E., Baer, L. A. & Ronca, A. E. Effects of hypergravity on mammary metabolic function: gravity acts as a continuum. *J. Appl. Physiol.* **95**, 2350–2354 (2003). [DOI] [PubMed] [Google Scholar]

23. Tuday, E. C., Nyhan, D., Shoukas, A. A. & Berkowitz, D. E. Simulated microgravity-induced aortic remodeling. *J. Appl. Physiol.* **106**, 2002–2008 (2009). [DOI] [PMC free article] [PubMed] [Google Scholar]

24. Tuday, E. C., Meck, J. V., Nyhan, D., Shoukas, A. A. & Berkowitz, D. E. Microgravity-induced changes in aortic stiffness and their role in orthostatic intolerance. *J. Appl. Physiol.* **102**, 853–858 (2007). [DOI] [PubMed] [Google Scholar]

25. Arbeille, P., Provost, R. & Zuj, K. Carotid and femoral arterial wall distensibility during long-duration spaceflight. *Aerosp. Med. Hum. Perform.* **88**, 924–930 (2017). [DOI] [PubMed] [Google Scholar]

26. Rabineau, J. et al. Cardiovascular deconditioning and impact of artificial gravity during 60-day head-down bed rest-Insights from 4D flow cardiac MRI. *Front. Physiol.* **13**, 944587 (2022). [DOI] [PMC free article] [PubMed] [Google Scholar]

27. Boutouyrie, P. et al. Aortic stiffness is an independent predictor of primary coronary events in hypertensive patients. *Hypertension* **39**, 10–15 (2002). [DOI] [PubMed] [Google Scholar]

28. Blacher, J. et al. Carotid arterial stiffness as a predictor of cardiovascular and all-cause mortality in end-stage renal disease. *Hypertension* **32**, 570–574 (1998). [DOI] [PubMed] [Google Scholar]

29. Laurent, S. et al. Aortic stiffness is an independent predictor of all-cause and cardiovascular mortality in hypertensive patients. *Hypertension* **37**, 1236–1241 (2001). [DOI] [PubMed] [Google Scholar]

30. Mitchell, G. F. et al. Arterial stiffness and cardiovascular events. *Circulation* **121**, 505–511 (2010). [DOI] [PMC free article] [PubMed] [Google Scholar]

31. Whitaker, A. A. et al. Lower middle cerebral artery blood velocity during low-volume high-intensity interval exercise in chronic stroke. *J. Cereb. Blood Flow Metab*. **44**, 627–640 (2024). [DOI] [PMC free article] [PubMed] [Google Scholar]

32. Brumback, L. C. et al. The association between arterial compliance, as assessed by PTC1 and PTC2 from radial artery waveforms, and age, sex, and race/ethnicity. *J. Hypertens.* **41**, 1117–1126 (2023). [DOI] [PMC free article] [PubMed] [Google Scholar]

33. Angoff, R., Mosarla, R. C. & Tsao, C. W. Aortic stiffness: epidemiology, risk factors, and relevant biomarkers. *Front. Cardiovasc. Med.* **8**, 709396 (2021). [DOI] [PMC free article] [PubMed]

34. Tomiyama, H. et al. Influences of age and gender on results of noninvasive brachial-ankle pulse wave velocity measurement—a survey of 12517 subjects. *Atherosclerosis* **166**, 303–309 (2003). [DOI] [PubMed] [Google Scholar]

35. Rossi, P., Francès, Y., Kingwell, B. A. & Ahimastos, A. A. Gender differences in artery wall biomechanical properties throughout life. *J. Hypertens.* **29**, 1023–1033 (2011). [DOI] [PubMed] [Google Scholar]

36. Regitz-Zagrosek, V. & Kararigas, G. Mechanistic pathways of sex differences in cardiovascular disease. *Physiol. Rev.* **97**, 1–37 (2017). [DOI] [PubMed] [Google Scholar]

37. Kuhn, E. R., Bellon, K., Huybrechts, L. & Heyns, W. Endocrine differences between the Wistar and

Sprague-Dawley laboratory rat: influence of cold adaptation. *Horm. Metab. Res.***15**, 491–498 (1983). [DOI] [PubMed] [Google Scholar]

38. Sanchís-Ollé, M. et al. Male long-Evans rats: an outbred model of marked hypothalamic-pituitary-adrenal hyperactivity. *Neurobiol. Stress***15**, 100355 (2021). [DOI] [PMC free article] [PubMed] [Google Scholar]

39. Möstl, S. et al. Limited effect of 60-days strict head down tilt bed rest on vascular aging. *Front. Physiol.***12**, (2021). [DOI] [PMC free article] [PubMed]

40. Hoffmann, B. et al. Mechanical deconditioning of the heart due to long-term bed rest as observed on seismocardiogram morphology. *npj Microgravity***8**, 25 (2022). [DOI] [PMC free article] [PubMed] [Google Scholar]

41. Boutouyrie, P. et al. Impact of 60 days of head-down bed rest on large arteries. *J. Hypertens.***40**, 2058–2067 (2022). [DOI] [PubMed] [Google Scholar]

42. Lopez-Candales, A. & Hernandez-Suarez, D. F. Strain imaging echocardiography: what imaging cardiologists should know. *Curr. Cardiol. Rev.***13**, 118–129 (2017). [DOI] [PMC free article] [PubMed] [Google Scholar]

43. Cauwenberghs, N. et al. Doppler indexes of left ventricular systolic and diastolic function in relation to the arterial stiffness in a general population. *J. Hypertens.***34**, 762–771 (2016). [DOI] [PubMed] [Google Scholar]

44. Kaess, B. M. et al. Relations of central hemodynamics and aortic stiffness with left ventricular structure and function: the Framingham Heart Study. *J. Am. Heart Assoc.***5**, e002693 (2016). [DOI] [PMC free article] [PubMed] [Google Scholar]

45. Kim, H. L. et al. Association between arterial stiffness and left ventricular diastolic function in relation to gender and age. *Medicine***96**, e5783 (2017). [DOI] [PMC free article] [PubMed] [Google Scholar]

46. Russo, C. et al. Arterial stiffness and wave reflection. *Hypertension***60**, 362–368 (2012). [DOI] [PMC free article] [PubMed] [Google Scholar]

47. Delp, M. D., Holder-Binkley, T., Laughlin, M. H. & Hasser, E. M. Vasoconstrictor properties of rat aorta are diminished by hindlimb unweighting. *J. Appl. Physiol.***75**, 2620–2628 (1993). [DOI] [PubMed] [Google Scholar]

48. Papadopoulos, A. & Delp, M. D. Effects of hindlimb unweighting on the mechanical and structure properties of the rat abdominal aorta. *J. Appl. Physiol.***94**, 439–445 (2003). [DOI] [PubMed] [Google Scholar]

49. Mueller, P. J., Foley, C. M. & Hasser, E. M. Hindlimb unloading alters nitric oxide and autonomic control of resting arterial pressure in conscious rats. *Am. J. Physiol. Regul. Integr. Comp. Physiol.* **289**, R140–R147 (2005). [DOI   ] [PubMed] [Google Scholar   ]

50. Tsvirkun, D. et al. Contribution of social isolation, restraint, and hindlimb unloading to changes in hemodynamic parameters and motion activity in rats. *PLoS ONE* **7**, e39923 (2012). [DOI   ] [PMC free article] [PubMed] [Google Scholar   ]

51. Johnson, R. T., Solanki, R. & Warren, D. T. Mechanical programming of arterial smooth muscle cells in health and ageing. *Biophys. Rev.* **13**, 757–768 (2021). [DOI   ] [PMC free article] [PubMed] [Google Scholar   ]

52. Locatelli, L., Castiglioni, S. & Maier, J. A. M. From cultured vascular cells to vessels: the cellular and molecular basis of vascular dysfunction in space. *Front. Bioeng. Biotechnol.* **10**, 862059 (2022). [DOI   ] [PMC free article] [PubMed] [Google Scholar   ]

53. Jiang, M. et al. Focal adhesions are involved in simulated-microgravity-induced basilar and femoral arterial remodelling in rats. *Can. J. Physiol. Pharm.* **96**, 772–782 (2018). [DOI   ] [PubMed] [Google Scholar   ]

54. Mozafari, H., Wang, L., Lei, Y. & Gu, L. Multi-scale modeling of the lamellar unit of arterial media. *Nanotechnol. Rev.* **8**, 539–547 (2019). [Google Scholar   ]

55. Dorta, M. P., de Brito, I. V., Pereira, A. C. & Alencar, A. M. Quantification of alignment of vascular smooth muscle cells. *Cytom. A* **93**, 533–539 (2018). [DOI   ] [PubMed] [Google Scholar   ]

56. Yi, B. et al. Stiffness of aligned fibers regulates the phenotypic expression of vascular smooth muscle cells. *ACS Appl. Mater. Interfaces* **11**, 6867–6880 (2019). [DOI   ] [PubMed] [Google Scholar   ]

57. Bose, P., Eyckmans, J., Nguyen, T. D., Chen, C. S. & Reich, D. H. Effects of geometry on the mechanics and alignment of three-dimensional engineered microtissues. *ACS Biomater. Sci. Eng.* **5**, 3843–3855 (2019). [DOI   ] [PubMed] [Google Scholar   ]

58. Barcus, C. E., Holt, E. C., Keely, P. J., Eliceiri, K. W. & Schuler, L. A. Dense collagen-I matrices enhance pro-tumorigenic estrogen-prolactin crosstalk in MCF-7 and T47D breast cancer cells. *PLoS ONE* **10**, e0116891 (2015). [DOI   ] [PMC free article] [PubMed] [Google Scholar   ]

59. Cocciolone, A. J. et al. Elastin, arterial mechanics, and cardiovascular disease. *Am. J. Physiol. Heart Circ. Physiol.* **315**, H189–H205 (2018). [DOI   ] [PMC free article] [PubMed] [Google Scholar   ]

60. Kehmeier, M. N. et al. In vivo arterial stiffness, but not isolated artery endothelial function, varies with the

mouse estrous cycle. *Am. J. Physiol. Heart Circ. Physiol.***323**, H1057–h1067 (2022). [DOI] [PMC free article] [PubMed] [Google Scholar]

61. Rosa-Caldwell, M. E. et al. Influence of gonadectomy on muscle health in micro- and partial-gravity environments in rats. *J. Appl. Physiol.***134**, 1438–1449 (2023). [DOI] [PMC free article] [PubMed] [Google Scholar]

62. Peter, I. et al. Association between arterial stiffness and variations in oestrogen-related genes. *J. Hum. Hypertens.***23**, 636 (2009). [DOI] [PMC free article] [PubMed] [Google Scholar]

63. Holets, L. M. et al. STS-135: Space flight induces down-regulation of estrogen receptor alpha gene and Protein expression in mouse uterus and ovary, and new methods for tissue storage and RNA/protein harvesting suitable for ISS Tissue dissection/fixation in flight. In *American Society for Gravitational and Space Research*, New Orleans, LA (2012).

64. Groban, L. et al. Female heart health: is GPER the missing link? *Front. Endocrinol.***10**, (2020). [DOI] [PMC free article] [PubMed]

65. Prossnitz, E. R. & Barton, M. The G-protein-coupled estrogen receptor GPER in health and disease. *Nat. Rev. Endocrinol.***7**, 715–726 (2011). [DOI] [PMC free article] [PubMed] [Google Scholar]

66. Kilanowski-Doroh, I. M. et al. Ovariectomy-induced arterial stiffening differs from vascular aging and is reversed by GPER activation. *Hypertension***81**, e51–e62 (2024). [DOI] [PMC free article] [PubMed] [Google Scholar]

67. Ogola, B. O. et al. Sex and the G protein-coupled estrogen receptor impact vascular stiffness. *Hypertension***78**, e1–e14 (2021). [DOI] [PMC free article] [PubMed] [Google Scholar]

68. Liu, L. et al. GPER activation ameliorates aortic remodeling induced by salt-sensitive hypertension. *Am. J. Physiol. Heart Circ. Physiol.***310**, H953–H961 (2016). [DOI] [PMC free article] [PubMed] [Google Scholar]

69. Wang, H. et al. Activation of GPR30 attenuates diastolic dysfunction and left ventricle remodelling in oophorectomized mRen2.Lewis rats. *Cardiovasc. Res.***94**, 96–104 (2012). [DOI] [PMC free article] [PubMed] [Google Scholar]

70. Lindsey, S. H., Yamaleyeva, L. M., Brosnihan, K. B., Gallagher, P. E. & Chappell, M. C. Estrogen receptor GPR30 reduces oxidative stress and proteinuria in the salt-sensitive female mRen2.Lewis rat. *Hypertension***58**, 665–671 (2011). [DOI] [PMC free article] [PubMed] [Google Scholar]

71. Meyer, M. R., Field, A. S., Kanagy, N. L., Barton, M. & Prossnitz, E. R. GPER regulates endothelin-

dependent vascular tone and intracellular calcium. *Life Sci.***91**, 623–627 (2012). [DOI   ] [PMC free article] [PubMed] [Google Scholar   ]

72. Meyer, M. R. et al. Deletion of G protein-coupled estrogen receptor increases endothelial vasoconstriction. *Hypertension***59**, 507–512 (2012). [DOI   ] [PMC free article] [PubMed] [Google Scholar   ]

73. Davis, K. E. et al. Sexually dimorphic role of G protein-coupled estrogen receptor (GPER) in modulating energy homeostasis. *Horm. Behav.***66**, 196–207 (2014). [DOI   ] [PMC free article] [PubMed] [Google Scholar   ]

74. Mårtensson, U. E. A. et al. Deletion of the G protein-coupled receptor 30 impairs glucose tolerance, reduces bone growth, increases blood pressure, and eliminates estradiol-stimulated insulin release in female mice. *Endocrinology***150**, 687–698 (2009). [DOI   ] [PubMed] [Google Scholar   ]

75. Reidy, P. T., Monnig, J. M., Pickering, C. E., Funai, K. & Drummond, M. J. Preclinical rodent models of physical inactivity-induced muscle insulin resistance: challenges and solutions. *J. Appl. Physiol.***130**, 537–544 (2021). [DOI   ] [PMC free article] [PubMed] [Google Scholar   ]

76. Prossnitz, E. R. & Barton, M. Estrogen biology: new insights into GPER function and clinical opportunities. *Mol. Cell Endocrinol.***389**, 71–83 (2014). [DOI   ] [PMC free article] [PubMed] [Google Scholar   ]

77. Valavanidis, A., Vlachogianni, T. & Fiotakis, C. 8-hydroxy-2' -deoxyguanosine (8-OHdG): a critical biomarker of oxidative stress and carcinogenesis. *J. Environ. Sci. Health C Environ. Carcinog. Ecotoxicol. Rev.***27**, 120–139 (2009). [DOI   ] [PubMed] [Google Scholar   ]

78. Singh, R., Rajput, M. & Singh, R. P. Simulated microgravity triggers DNA damage and mitochondria-mediated apoptosis through ROS generation in human promyelocytic leukemic cells. *Mitochondrion***61**, 114–124 (2021). [DOI   ] [PubMed] [Google Scholar   ]

79. Qiong, W. et al. The memory enhancement effect of Kai Xin San on cognitive deficit induced by simulated weightlessness in rats. *J. Ethnopharmacol.***187**, 9–16 (2016). [DOI   ] [PubMed] [Google Scholar   ]

80. Di Minno, A. et al. 8-Hydroxy-2-deoxyguanosine levels and cardiovascular disease: a systematic review and meta-analysis of the literature. *Antioxid. Redox Signal***24**, 548–555 (2016). [DOI   ] [PMC free article] [PubMed] [Google Scholar   ]

81. Kotani, K. & Yamada, T. Association between urinary 8-OHdG and pulse wave velocity in hypertensive patients with type 2 diabetes mellitus. *Singap. Med. J.***55**, 202–208 (2014). [DOI   ] [PMC free article] [PubMed] [Google Scholar   ]

82. Lawler, J. M., Song, W. & Demaree, S. R. Hindlimb unloading increases oxidative stress and disrupts antioxidant capacity in skeletal muscle. *Free Radic. Biol. Med.* **35**, 9–16 (2003). [DOI] [PubMed] [Google Scholar]

83. Martins, S. G., Zilhão, R., Thorsteinsdóttir, S. & Carlos, A. R. Linking oxidative stress and DNA damage to changes in the expression of extracellular matrix components. *Front. Genet.* **12**, 673002 (2021). [DOI] [PMC free article] [PubMed] [Google Scholar]

84. Xu, J. et al. Anti-inflammatory actions of G-protein-coupled estrogen receptor 1 (GPER) and brain-derived estrogen following cerebral ischemia in ovariectomized rats. *Biology* **12**, 99 (2023). [DOI] [PMC free article] [PubMed] [Google Scholar]

85. Singh, A. P., Singh, N. & Singh Bedi, P. M. Estrogen attenuates renal IRI through PPAR-gamma agonism in rats. *J. Surg. Res.* **203**, 324–330 (2016). [DOI] [PubMed] [Google Scholar]

86. Tiyerili, V. et al. Estrogen improves vascular function via peroxisome-proliferator-activated-receptor-gamma. *J. Mol. Cell Cardiol.* **53**, 268–276 (2012). [DOI] [PubMed] [Google Scholar]

87. Sato, H. et al. Sex hormones influence expression and function of peroxisome proliferator-activated receptor gamma in adipocytes: pathophysiological aspects. *Horm. Mol. Biol. Clin. Investig.* **20**, 51–61 (2014). [DOI] [PubMed] [Google Scholar]

88. Yamaleyeva, L. M., Elsangeedy, E., Willey, J. S. & Pulgar, V. M. Sex Differences In Aortic Stiffness Following Simulated Microgravity In Middle Aged Rats. *Hypertension.* **76**, 10.1161/hyp.76.suppl_1.P078 (2020).

89. Fang, S., Livergood, M. C., Nakagawa, P., Wu, J. & Sigmund, C. D. Role of the peroxisome proliferator activated receptors in hypertension. *Circ. Res.* **128**, 1021–1039 (2021). [DOI] [PMC free article] [PubMed] [Google Scholar]

90. Chen, J.-Y. et al. PPARγ activation improves the microenvironment of perivascular adipose tissue and attenuates aortic stiffening in obesity. *J. Biomed. Sci.* **28**, 22 (2021). [DOI] [PMC free article] [PubMed] [Google Scholar]

91. Prisby, R. D. et al. Endothelium-dependent vasodilation of cerebral arteries is altered with simulated microgravity through nitric oxide synthase and EDHF mechanisms. *J. Appl. Physiol.* **101**, 348–353 (2006). [DOI] [PubMed] [Google Scholar]

92. Tahimic, C. G. T. & Globus, R. K. Redox signaling and its impact on skeletal and vascular responses to spaceflight. *Int. J. Mol. Sci.* **18**, 2153 (2017). [DOI] [PMC free article] [PubMed] [Google Scholar]

93. Willey, J. S. et al. Spaceflight-relevant challenges of radiation and/or reduced weight bearing cause arthritic responses in knee articular cartilage. *Radiat. Res.* **186**, 333–344 (2016). [DOI] [PubMed] [Google Scholar]

94. Lindsey, S. H., Cohen, J. A., Brosnihan, K. B., Gallagher, P. E. & Chappell, M. C. Chronic treatment with the G protein-coupled receptor 30 agonist G-1 decreases blood pressure in ovariectomized mRen2.Lewis rats. *Endocrinology* **150**, 3753–3758 (2009). [DOI] [PMC free article] [PubMed] [Google Scholar]

95. Bredfeldt, J. S. et al. Computational segmentation of collagen fibers from second-harmonic generation images of breast cancer. *J. Biomed. Opt.* **19**, 16007 (2014). [DOI] [PMC free article] [PubMed] [Google Scholar]

96. Yamaleyeva, L. M. et al. Uterine artery dysfunction in pregnant ACE2 knockout mice is associated with placental hypoxia and reduced umbilical blood flow velocity. *Am. J. Physiol. Endocrinol. Metab.* **309**, E84–E94 (2015). [DOI] [PMC free article] [PubMed] [Google Scholar]

97. Westwood, B. M. & Chappell, M. C. Application of correlate summation to data clustering in the estrogen- and salt-sensitive female MREN2.Lewis rat. In *Proceedings of the 1st international workshop on Text mining in bioinformatics (TMBIO '06)*. 21-26 (Association for Computing Machinery, New York, NY, USA, 2006).

Associated Data

This section collects any data citations, data availability statements, or supplementary materials included in this article.

Supplementary Materials

Supplementary material (232.4KB, pdf)

Data Availability Statement

The data that support the findings of this study are available in "Methods", "Results", "Discussion" and/or Supplementary Material of this article.